Characterisation of long range radiation heat transfer in packed pebble beds

MOKGWASI LUCAS PITSO

12619825

Dissertation submitted in partial fulfilment of the requirements of the degree Magister Engeneriae at the North-West University

Supervisor: **Prof. PG Rousseau**

Co -Supervisor: **Prof. CG du Toit**

November 2011

Abstract

Name: Lucas Pitso

Title: Characterisation of long range radiation heat transfer in packed pebble beds

Date: November 2011

Due to its importance in the safety case of high temperature gas-cooled nuclear reactors, the effective thermal conductivity in packed pebble beds has been extensively studied by various researchers and several correlations have been developed. The correlations, mostly based on a unit cell approach, can model the total heat transfer through packed beds with reasonable accuracy.

However, these correlations are typically highly empirical and do not discriminate between short and long-range radiation phenomena. It therefore does not specifically address the long-range radiation in detail at higher temperatures and in cases with large temperature gradients through the bed. It also does not discriminate between the pebble-to-pebble radiation in the bulk region and the pebble-to-reflector radiation in the near-wall regions. Long range radiation in such cases becomes important and it greatly influences the temperature distribution and heat flux. A need therefore arose to study long range radiation in packed pebble beds in more detail.

Using the Computational Fluid Dynamics (CFD) program Star-CCM+, different unstructured and structured beds were studied in an effort to characterise the long range radiation phenomenon. Long range radiation in the bulk regions and near-wall regions of the beds was quantified through the use of view factors. Based on data from the characterisation of long range radiation, a new model is proposed in which long range radiation is simplified and predicted through a so-called Spherical Unit Nodalization (SUN) approach. This model was validated using CFD.

The new model can now form the basis for the development of a specific term in the effective thermal conductivity which may be used in correlations to represent the effects of long range radiation in more detail.

Acknowledgements

I immensely thank my supervisors, Prof. Rousseau and Prof. du Toit, for the guidance they provided during the course of the study. Also Werner van Antwerpen, on whose work parts of this study is based and thanks for all the information you provided. I thank my parents and two brothers for all the love and support that they've always provided me with.

Table of contents

List of Figures

List of Tables

Nomenclature

Abbreviation	Definition
A.I.Ch.E.	American Institute of Chemical Engineers
BEM	Boundary Element Method
CFD	Computation Fluid Dynamics
D	Dimensional
DOM	Discrete Ordinates Method
FDM	Finite Difference Method
FEM	Finite Element Method
EES	Engineering Equation Solver
HTGR	High Temperature Gas Reactor
HTTU	High Temperature Test Unit
MSUC	Multi-Sphere Unit Cell
PBMR	Pebble Bed Modular Reactor
PBR	Pebble Bed Reactor
RTC	Radiative Transfer Coefficient
RTE	Radiative Transfer Equation
SANA	Selbstätige Abfuhr der NAchwärme
SUN	Spherical Unit Nodalization
TRISO	TRistructural-ISOtropic
ZBS	Zehner, Bauer and Schlünder
Variable	**Definition**
A_i	Area of surface i, m^2
d, d_p	Diameter of a sphere, m
E_b	Total emissive power of surface if it was a blackbody, W / m^2
f_k	Non-isothermal correction factor
F_{ij}	View factor from surface i to surface j
F_E^*	Radiation exchange factor

$F_{1-2,avg}^{L}$	Average long range view factor
J	Radiosity, W/m^2
$L_{r,avg}$	Average long range geometrical length, m
k	Thermal conductivity
k_g	Thermal conductivity for gas phase, $W/m-K$
k_s	Thermal conductivity for solid phase, $W/m-K$
k_e^r	Effective radiative thermal conductivity, $W/m-K$
q_{ij}, Q_{12}	Heat flux from surface $i,1$ to surface $j,2$, W
$Q_{i,rad}$	Radiation heat flux between surface i and its environment, W
T	Temperature, K
$\overline{T}$	Average bed temperature, K
$T_{local,i}$	Local averaged temperature of the spheres and fluid, K
z_i	Distance
Greek Symbols	**Definition**
ε_r, ε_{pi}	Emissivity
σ	Stephan-Boltzmann constant, $\sigma = 5.67\times10^{-8}\ W/m^2-K^4$
Subscripts	**Definition**
c	Cold
f	Fluid
g	Gas
h	Hot
i	Pebble, surface or sphere i, increment
j	Pebble, surface or sphere i, increment
s	Solid

1. Introduction

1.1 BACKGROUND OF THE STUDY

Research into gas-cooled reactors that can attain high temperatures has been on-going since World War II (Lamarsh and Baratta, 2001). In the early days of nuclear power development, Britain and France adopted gas-cooled, closed cycle systems for their reactors which used carbon dioxide as the coolant gas. The use of gas offered better containment and control as the gas minimises neutron absorption. Thus radioactivity in the gas was low. Gas-cooled reactors have a much higher thermal efficiency as they can be operated at higher temperatures than light water reactors. They are capable of producing superheated steam whereas most water-cooled reactors can only produce saturated steam.

The United States favoured light water reactors and they went on to become the dominant reactors for power generation. Gas-cooled reactors could not compete on price and thus their development was greatly hampered. Two major accidents on light water reactors, Chernobyl and Three Mile Island, and several smaller accidents have however raised safety concerns with regards to nuclear power. Nicholls (2000) stated that safety was one of the very serious considerations when Eskom, the South African power utility, decided to embark on a nuclear programme. Eskom then decided on the Pebble Bed Modular Reactor (PBMR), which is a high temperature gas-cooled reactor (HTGR). Koster *et al.* (2002) listed the features of the PBMR reactor. HTGRs are seen worldwide as one of the next generation type reactors in nuclear power development due to their inherent safety features.

One of the safety features of an HTGR is that should the reactor suddenly shut-down, all decay heat will be transferred to the vessel wall of the reactor and will be lost to the atmosphere through convection, in the absence of active cooling systems. The core of some HTGR reactors consists of pebbles that will be randomly packed. These pebbles contain the fuel and through interactions with neutrons they generate heat. A coolant, usually gas such as carbon dioxide or helium, circulates through the bed to extract the heat so that it may be used in power generation. Should a reactor shut-down, these pebbles will remain at high temperatures and the heat needs to be removed to prevent overheating of the core. It was experimentally proven at the SANA experiments (Breitbach and Barthels, 1980) that passive safety mechanisms, where heat is transferred to the walls of the reactor vessel, are valid and can be used effectively. This however, requires that heat transfer within a pebble bed be fully understood in order to predict the effectiveness of such systems.

1.2 PROBLEM STATEMENT

Heat transfer within packed pebble beds has been extensively studied and several correlations have been developed. These correlations, for effective thermal conductivity, can with relative accuracy, predict heat transfer in pebble beds at medium temperatures. However at high temperatures (>1000 °C), the predictions by the correlations differ by significant margins from experimental data. At such temperatures, radiation is the dominant heat transfer mechanism, which these correlations do not model very accurately.

In addition to radiation heat transfer at high temperatures, the pebble-to-reflector region is another area at which heat transfer has not been explored extensively. A major assumption has been to attempt to predict heat transfer in the wall regions by using the same correlations as those for the bulk region. However, some authors have shown that in the SANA experiments the heat transfer in the near-wall regions differed from heat transfer in the pebble regions and that can clearly be seen in the temperature distribution profiles.

None of the models developed thus far pay specific attention to the near-wall regions (Van Antwerpen *et al.*, 2010), except for the Multi-Sphere Unit Cell Model developed by van Antwerpen. Furthermore, there is very little experimental data at high temperatures available in open literature from which to develop specific models.

1.3 AIM OF THE STUDY

The aim of this study was to characterise the long range radiation heat transfer from a single sphere towards all other spheres in a randomly packed pebble bed. The characterisation had to be done in such a way that it can be used to derive a simplified model which may be used as part of a larger model for the total effective thermal conductivity. Such a model for the long range radiation would then be derived and tested by comparing its results with that of a detailed CFD simulation model.

1.4 METHODOLOGY

The radiative heat exchange (q_{ij}) between two surfaces which may be approximated as blackbodies is defined as:

$$q_{ij} = A_i F_{ij} \sigma (T_i^4 - T_j^4) \tag{1.1}$$

where F_{ij} is the view factor. This view factor represents the proportion of all radiation leaving surface i that is intercepted by surface j. The view factors in Equation (1.1) is a geometrical property which may be used to determine the distribution of radiation from a single sphere to all other spheres within

a packed pebble bed and is therefore used as the basis from which to characterise the long range radiation. This was done by extracting the calculated view factors from a Computational Fluid Dynamics (CFD) software model in Star-CCM+ for a representative section of a randomly packed bed. Based on data from this characterisation, a simplified model for radiation heat transfer was then developed and programmed in Engineering Equation Solver (EES). Finally, the new model was tested by comparing its results with that of the CFD simulation.

1.5 CONTRIBUTIONS OF THE STUDY

The first major contribution of this study is the characterisation of the distribution of radiation heat transfer within a pebble bed from a single sphere. The extent and impact of long range radiation is also shown, which proves that the effects of long range radiation must be considered in any correlation which attempts to predict effective heat transfer within packed beds.

The second contribution is a simplified model for radiation heat transfer within packed beds, named the Spherical Unit Nodalization (SUN) Model. This model makes use of the characterisation of radiation heat transfer, as well as the concept of discretization to predict the long range radiation heat transfer in packed pebble beds.

1.6 CHAPTER OUTLINE

Following this chapter, Chapter 2 presents the theoretical models for effective thermal conductivity. It also presents typical experimental techniques for determining effective thermal conductivity. Literature on radiation in packed beds is then briefly discussed, and the chapter concludes with the limitations of previous studies on pebble beds particularly relating to radiation heat transfer.

Chapter 3 discusses the fundamentals of radiation heat transfer in packed beds. The hypothesis for radiation heat transfer in packed pebble beds, which is the basis for the Spherical Unit Cell model, is presented afterwards.

The hypothesis is tested in Chapter 4. The outcomes of characterisation of radiation are presented here. Presented in this chapter as well are the methodology, parameters and boundaries of the test, whose results are shown in Chapter 5. The study is summarised in Chapter 6 which also includes the conclusions.

2. Heat Transfer in Randomly Packed Beds

2.1 BACKGROUND

A Pebble Bed Reactor (PBR) is one type of design, as opposed to the "prismatic block" core reactor, for HTGRs which is graphite moderated and cooled by an inert or semi-inert gas, such as helium, nitrogen or carbon dioxide. The base of this design is pebbles, which are spherical fuel elements that are roughly the size of a tennis ball. These graphite pebbles contain thousands of micro fuel particles called TRISO (Tristructural-isotropic) particles. It is within these TRISO particles that the fissile material such as ^{235}U, in the form of UO_2, coated with silicon carbide and carbon for structural integrity and containment of fission products, is found. A PBR requires thousands of these pebbles to form a nuclear reactor core (Wikipedia, 2011).

During fission chain reactions, heat is released from the TRISO particles. This heat is removed by the gas flowing over the pebbles, typically raising the gas temperature up to 850 °C. The gas can in turn be used to generate steam, or drive power-generating turbines. The transport of heat from the TRISO particles to the gas is complex and there are a number of heat transfer mechanisms acting simultaneously. The two primary directions of heat transfer in the core are (1) axially – mainly due to forced convection by the flowing gas and (2) radially. Heat transfer in the radial direction is due to a combination of various heat transfer mechanisms. Van Antwerpen (2009) illustrated these mechanisms, which include:

1. Conduction through the solids,
2. Conduction through the contact area between adjacent spheres,
3. Conduction through the fluid phase,
4. Thermal radiation between spheres in contact with one another (short range radiation) and spheres not in contact with one another (long range radiation).

The overall heat transfer in the radial direction is characterised by a so-called effective thermal conductivity, which represents the net effect of all the modes of transport.

2.2 THEORETICAL MODELS FOR EFFECTIVE THERMAL CONDUCTIVITY

Zehner and Schlünder (1970) developed a unit cell model to predict the effective thermal conductivity through a pebble bed. Pebble beds of any shape and size can theoretically be analysed with this model. The bed is represented by a unit cell, which is two half-spheres facing each other. Van Antwerpen *et al* (2010) notes that Bauer later improved this model to include thermal radiation and to account for heat transfer through contact areas The improved model came to be known as the Zehner,

Bauer and Schlünder (ZBS) model and it is widely used and commonly referenced in the nuclear industry.

When developing a systems CFD model for a packed bed of a HTGR, du Toit *et al.* (2006) implemented the Zehner-Schlünder model within Flownex® (van der Merwe & van Ravenswaay, 2003) to determine the effective thermal conductivity for heat transfer between the pebbles. They found that the Zehner-Schlünder model's predictions matched the SANA experimental data with sufficient accuracy over the full range of temperatures in the bulk region.

However, a deviation was observed in the near wall region, where the model was not conservative and therefore under-predicted the temperatures. Du Toit *et al.* attributed this to the inability of the Zehner-Schlünder model to distinguish between heat transfer in the bulk region, where it is primarily pebble-to-pebble, and heat transfer in the near wall region, where it is primarily pebble-to-wall.

Other models have also been developed and adopted. Okazaki *et al.* (1981) presented a model, also a unit cell, which considers a number of other factors, including number of contact points, sphere packing and heat flow per contact. Kunii and Smith (1960) presented a model in which the fluid is stagnant. Their model assumes heat transfer to be in the vertical direction. Torquato (1987) provided a statistical model which agrees very well with experimental data, as long as the ratio of solid material heat conductivity to gas thermal conductivity k_s / k_g is kept low. Numerous other authors have published their own correlations, including Bahrami *et al.* (2006) and Slavin *et al.* (2002).

The correlations mentioned above are useful, but not totally accurate in predicting the effective conductivity in pebble beds. As noted by Vortmeyer (as quoted by Van Antwerpen, 2009) the majority of these correlations ignore the effects of thermal radiation. When studying heat transfer in packed beds, Balakrishnan & Pei (1979) emphasized the importance of including the radiative effects where temperatures above 400 K are expected. They found that at temperatures of about 950 K, the contribution from radiation is almost equal to that of conduction, and increases rapidly beyond that. Chen and Churchill (1963) quoted Schotte to have found this contribution to be as high as 80 % in some cases.

Some authors tried to include the effects of radiation through introduction of the so-called radiative thermal conductivity, which is defined as:

$$k_e^r = 4F_E^* \sigma d_p \overline{T}^3 \tag{2.1}$$

where F_E^* is the radiation exchange factor, σ is the Stefan-Boltzmann constant and d_p is the diameter of the sphere. This method is prone to error because:

- It only remains valid if the steady state temperature drop ΔT across the local average bed dimension is much smaller than the average bed temperature, $\overline{T}$. i. e. $\Delta T / \overline{T} \leq 1$.
- The radiation exchange factor cannot be determined easily, although it is known that it is heavily dependent on the solid thermal conductivity k_s and the pebble emissivity ε_r.

Van Antwerpen *et al.* (2010) demonstrated the difference between the radiation exchange factor models and empirical data (See Figure 2.1). They concluded that this aspect should be studied in greater depth.

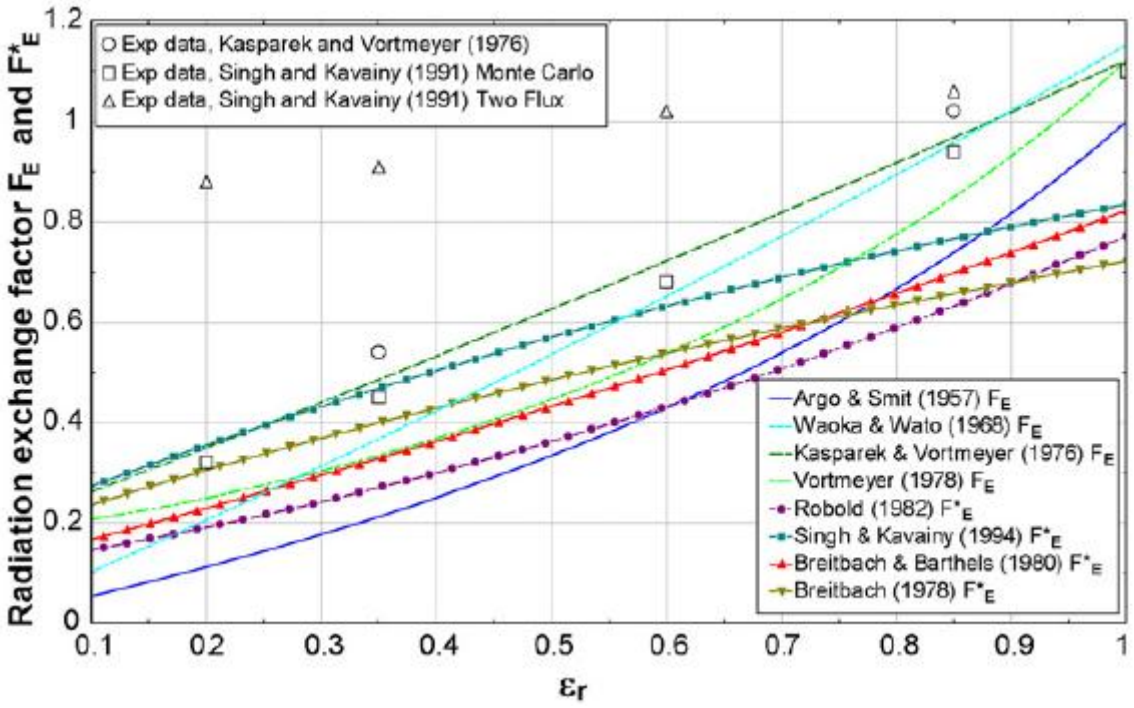

Figure 2.1: Comparison of radiation exchange models with experimental data.

In their study, Zhou *et al.* (2010) simplified the thermal radiation component of their model. They defined the heat flux due to radiation between the particle and its environment as

$$Q_{i,rad} = \sigma \varepsilon_{pi} A_i (T_{local,i}^4 - T_i^4) \tag{2.2}$$

where A_i is the area of surface i, ε_{pi} is the emissivity, and T_i is its temperature whilst $T_{local,i}$ is the averaged temperature of all other particles and the fluid. This is an extreme simplification as they consider all matter surrounding a particle to be a body at a single uniform temperature, with a view factor of unity, and ignore the thermal radiation among the particles themselves. They argued that

radiation is insignificant when the bed temperature is low. They acknowledged though that thermal radiation becomes significant when the bed temperatures exceeded 500 °C. In their simulations, the temperature at the bottom and top of the bed varied from 75 °C to 1475 °C, although the temperature difference between the bottom and top layers were kept at a constant 100 °C.

There are other methods which have been developed to determine radiative heat transfer in packed beds. The first, the Radiative Transfer Equation (RTE), is a balance equation for all media participating in the radiation exchange (Van Antwerpen, 2009). In order to solve the distribution of the radiation intensity, a number of optical properties must be obtained prior to the calculation. These optical properties are unique to each packing, and must be obtained either experimentally or numerically. This is turn has limited the further development and wider application of this method.

The second method is the Radiative Transfer Coefficient (RTC), developed by Lee *et al.* as quoted by Van Antwerpen (2009). It is numerical, and in it, a set of algebraic equations are established to determine the energy within each sphere. With the energies known, the temperature of each sphere can then be determined. The Monte Carlo ray-tracing method is used to calculate the RTC, and the equations are solved iteratively. These are its major drawbacks for it to be widely implemented.

Zhou *et al.* (2007) made use of advances in CFD and numerical methods to develop an effective conductivity model, which they named the Boundary Element Method (BEM). They proposed that the temperature field in the bed can be obtained by solving conduction differential equations in the solid and liquid phases and a heat flux boundary condition at the solid-fluid interfaces. The effective thermal conductivity could then be determined from the temperature field. Implementing this with common numerical methods would have been very taxing on computer memory. This is because it is complicated to adapt the Finite Difference Method (FDM) to complex geometries and the Finite Element Method (FEM) would require a very fine mesh. They thus developed their own numerical method, the 'boundary-only method' which converts the partial differential equations into boundary integral equations. Thus only boundary discretization is required. Due to the complex nature of randomly packed beds, the model is currently limited to square and hexagonal arrays.

To account for radiation, the model assumes that the solids are opaque and that the surfaces are diffuse and gray. The model also limits the calculation of radiation to the four convex solid surfaces of a fluid void in a square array, and ignores all neighbouring surfaces surrounding the fluid void. In essence, the model only computes short-range radiation. Radiation from one fluid void to another, which is a long range effect, was considered too complex by the authors. This iteratively solved model, despite its limitations, proved useful in studying effects of mean bed temperature, particle size and surface emissivity on the effective thermal conductivity.

The limitations of heat transfer correlations at the pebble bed-reflector interface were also studied by van der Merwe *et al.* (2006). They concluded that the correction factor proposed for effective conductivity in this region must be studied more fundamentally.

Van Antwerpen (2009) sought to develop an all-encompassing correlation, which would take into account variables highlighted by other correlations, as well as correct their shortcomings. After a comprehensive study, he proposed the Multi-Sphere Unit Cell (MSUC) model, in which he developed the radiation model by considering the packing structure more fundamentally. The model compared very well with experimental data from the High Temperature Test Unit (HTTU), performing better than previous correlations. However, a number of anomalies within the radiation model that he developed have been noted.

Firstly, he derived the effective thermal conductivity term for short-range radiation based on the following equation for radiative heat exchange:

$$Q_{12} = \frac{\sigma(T_1^4 - T_2^4)}{\frac{1-\varepsilon_1}{\varepsilon_1} + \frac{1}{A_1 F_{12}} + \frac{1-\varepsilon_2}{\varepsilon_2}} \tag{2.3}$$

where F_{12} is the radiation view factor, ε is the emissivity for the j^{th} surface and A is the area of the emitting surface. Incropea and de Witt (2001) stipulated that Equation (2.3) may be used for any two diffuse, gray surfaces *that form an enclosure*. Thus the equation is a special case for two surfaces that are radiating and re-radiating heat exclusively. A sphere involved in short-range radiation will radiate to all the spheres immediately surrounding it, or touching it. It is well known that a coordination number, defined as the number of particles in contact with the particle under consideration, for any packing will at least exceed one.

The second anomaly is in the approach he took to derive the long range radiation term. The current author studied the distribution of view factors from a sphere under consideration to other spheres using Star-CCM+, and the results are shown Figure 2.2 below.

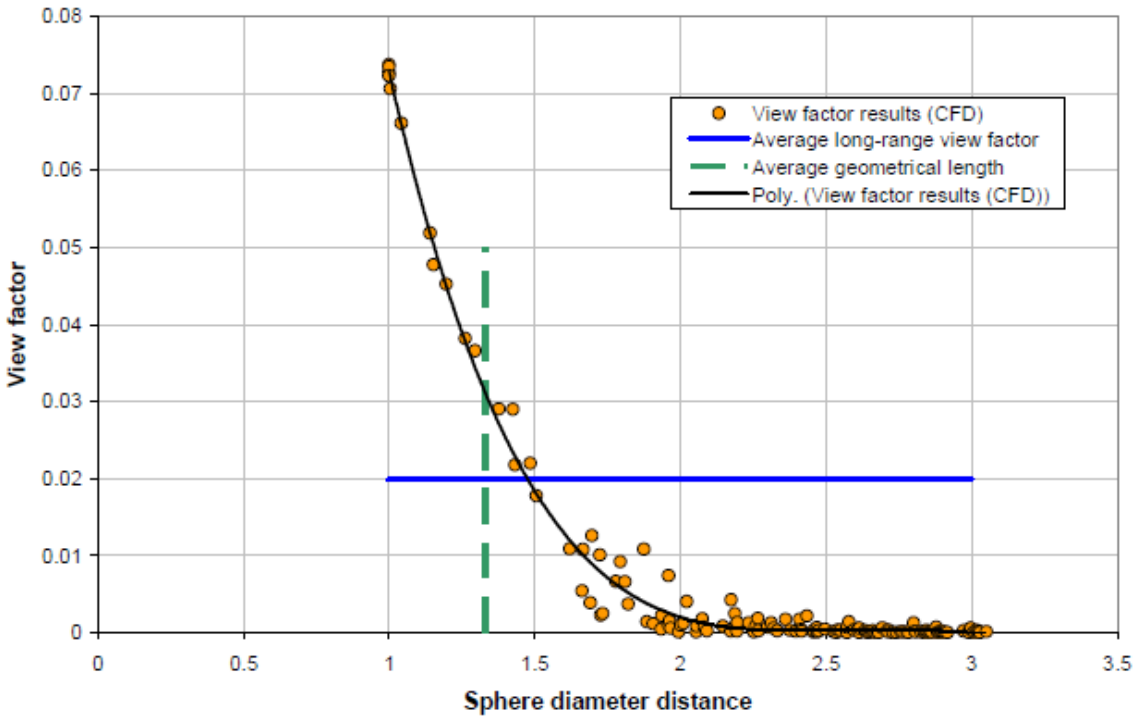

Figure 2.2: Long range diffuse view factors, as used by van Antwerpen (2009).

After establishing that the number of sphere diameters it would take to decrease the long-range view factor to zero is in the vicinity of $z_2 = 2.25$, Van Antwerpen (2009) fitted a polynomial to the view factor data from Figure 2.2. He then integrated this polynomial between a sphere diameter $(z_1 = 1)$ and to determine the average long range view factor, which he found to be $F^{L}_{1-2,avg} = 0.0199$. In a similar manner, he also established the average long range geometrical length, calculated to be $L_{r,avg} = 1.33 d_p$, d_p being the diameter of the sphere.

Using these derived variables, he proceeded to develop a term for effective thermal conductivity for long range radiation in a similar manner to the short range radiation term. The primary fault with this approach is that all the spheres that are not in contact with the sphere under consideration are lumped together, and viewed as a single surface. Their view factors from the sphere under consideration are averaged, which in itself is not wrong. However, the temperature of these spheres from thermal radiation would then be computed to be the same, even though from the shape of the graph in Figure 2.2, it can be seen that spheres closer to the under-study should be at a higher temperature. To enable to this term to match experimental data, Van Antwerpen introduced a non-isothermal correction factor, f_k. Data from simulations that he ran on Star-CCM+ was used to develop an equation to calculate this correction factor. But the data was only for short-range radiation, and the same

correction factor for short range radiation was also used for long range radiation. The use of this correction factor brings into question the applicability of the model to a wider range of use.

2.3 A LOOK AT EFFECTIVE THERMAL CONDUCTIVITY – EXPERIMENTALLY

Effective thermal conductivity has also been studied by some authors via experiments, and a few of the findings are discussed in the following paragraphs.

2.3.1 Linear Heat Transfer

When evaluating correlations for thermal conductivity, Prasad *et al.* (1989) set up an experimental facility in which heat conduction was linear. The apparatus was a plexiglass tube with solid aluminium plates at the bottom and top ends. The heat source was a thermo-foil heater of 15 Ω recessed within an acrylic plate. The aluminium plate at the bottom was cooler and had channels in it for water flow. It was also recessed in a plexi-glass plate. Temperature variations on the heater and cooler surfaces were monitored through radial thermocouples. The side walls of the apparatus were covered with insulation and the heat loss through the sides was not quantified. The temperature difference across the bed $T_h - T_c$ was varied between 10 and 50 °C and the cooling water was kept at constant room temperature. From the data obtained they were able to conclude that correlations by Kunii and Smith, Krupiczka and Zehner-Schlünder are valid as long as the ratio of k_f / k_s is less than unity.

Abou-Sena *et al.* (2007) measured the effective thermal conductivity of a bed packed with lithium titanate pebbles using an experimental apparatus. The pebbles, which were 1.7-2.0 mm in diameter, were packed in a bed which was heated at the top and cooled at the bottom. A ceramic cylinder which had a low thermal conductivity contained the pebbles to minimise heat loss through the sides. Thermocouples were placed along the heat path to determine the temperature profile. A heat flux meter was placed at the end alongside the cooling system. In this way, a 1-D heat transfer path could be created and by using Fourier's Law, the effective conductivity through the bed could be determined. They found the results to be in agreement with the model of Shapiro *et al.* (2004)'s model. However, the ZBS and Okazaki models over-predicted the effective conductivity at temperatures between 300 °C and 500 °C.

Effective conductivity is affected, although to a lesser extent, by the stress experienced by pebbles. Reimann *et al.* (2006) attempted to measure the effective thermal conductivity through a pebble bed when the pebbles were compressed. In their apparatus, a bed composed of pebbles was placed in-between two pistons. A 1-D temperature gradient was achieved through heaters placed at the top and bottom of the bed. Thermocouples were placed in radial positions (to ensure that heat transfer was

uniform) to determine the temperature profile across the height of the bed. As the bed was packed, the pebbles were shook to achieve a packing factor of 63.5 % (void fraction of 0.365). The test was conducted in a helium environment of 0.1 MPa and piston pressure > 0.3 MPa. The maximum temperature of the tests was 650 °C whilst the temperature differences were kept between 15 °C and 30 °C across the bed. From experimental data, they proposes a correlation $k = f(\varepsilon, T)$, where the conductivity is based on the ZBS model.

2.3.2 Radial Heat Transfer

An experimental set-up similar to the SANA experiments was used by Yagi and Kunii (1957) to obtain theoretical formulae for effective thermal conductivities. They packed the bed with different kinds of materials to determine the effect of packing material on the effective conductivity. The apparatus was a column with a coaxial heater. Thus there was a heater at the central column and at the side-reflector, to compensate for the heat loss. The pebbles were packed in the annulus. The temperature gradient was measured through thermocouples located at four radial positions. The air in the bed was considered to be stagnant. The temperature profiles that they obtained were relatively linear. One of their findings was that the pebble sizes greatly affect conductivity at high temperatures. For the larger pebbles packed randomly, the mean void length increases, this in turn increases heat radiation. High thermal conductivity of solids was also found to aid thermal radiation, and this was also observed by Zhou *et al.* (2007) in their study.

Most of the theoretical models are valid when solid-fluid conductivity ratio is low $(1 \le k_s / k_g < 10)$. Aichlmayr and Kulacki (2006) noted this and established that the effective conductivity is mostly dependent on the volume fractions and the thermal conductivities of the constituent phases at such low ratios. For moderate ratios $(10 \le k_s / k_g < 10^3)$, the effective conductivity is mildly sensitive, but there exists various ways to account for interface geometry. Effective conductivity is most sensitive to interface geometry when the ratio is high $(k_s / k_g \ge 10^3)$. Most PBRs have high solid-fluid conductivity ratios, simply because of the choice of materials for pebbles and the fluid used for cooling. This interface geometry as well as the larger solid conductivity will also affect thermal radiation.

When proposing a new analytical model that could be used for higher values of k_s / k_g, Slavin *et al.* (2000) constructed an experimental apparatus to validate this. The annulur shaped experiment had a heater with an external diameter of 19.1 mm at the centre. It was surrounded by alumina pebbles varying in diameter from 1 mm to 3 mm. The pebbles were cooled by helium gas flowing from bottom to top, whose pressure ranged from 0 to 100 kPa (No mention of whether pressure is absolute

or gauge). Thermocouples which were arranged radially measured the temperature profiles. The maximum temperatures measured were up to 700 K. The authors chose a length-to-diameter ratio of 5.7 to ensure that heat loss at the top and bottom would not influence the gradients obtained.

They included the effects of radiation in their model, and found that conduction through the points of contact was negligible compared to radiative transfer. They tested the transmissivity of the pebbles in question, and found that transmitted radiation fell to about 1 % after about 2 layers. Thus transmission and reflection of the radiation could not explain the large contribution. This might also suggest that there could be an error in the term that they used to account for the effects of radiation.

2.4 CONCLUSIONS FROM LITERATURE STUDY

The above literature has shown that there is a need to study thermal radiation in packed pebble beds in more detail. Of particular concern is that PBRs are intended to be operated at high temperatures, where radiation is the dominant heat transfer mechanism, yet the work that has been done thus far still cannot fully predict radiative heat transfer which is significant at higher temperature.

The existing effective thermal conductivity models for heat transfer in packed beds do not fully take thermal radiation into account. Those that attempts to, either do so through:

1. Introduction of empirical factors, which are not exact and are cumbersome to determine.
2. Use of methods which require significant computing power or resources to solve.
3. Limiting radiation to short-range radiation only.

It has also been shown that in the near wall region, the existing correlations fail to accurately predict heat transfer. Most of these correlations were developed for the bulk region of packed beds and do not take in account the change in the bed structure at regions close to the reflectors.

To date, the MSUC correlation by Van Antwerpen (2009) has proved to be accurate at high temperatures as well as at the near-wall region. However, the approach to develop its effective thermal conductivity term for long range radiation, although well-intended, is flawed and has broad simplifications and uncertainties. To be fair, Van Antwerpen did admit that it was a first approximation to the complex phenomenon of thermal radiation in packed beds.

2.5 ISSUES ADDRESSED

The aim of this study was to revisit thermal radiation more fundamentally. With the aid of the CFD software, Star-CCM+, thermal radiation was studied in more depth. The author proposed a simplified thermal radiation hypothesis, based on fundamental equations for radiation, and validated it.

3. Characterizing the Radiation Heat Transfer in Randomly Packed Beds

3.1 FUNDAMENTALS OF RADIATION HEAT TRANSFER

The net radiative exchange between two blackbody surfaces of any arbitrary shape is calculated as follows:

$$q_{ij} = A_i F_{ij} \sigma (T_i^4 - T_j^4) \tag{3.1}$$

A blackbody is however, an idealised object. In reality, surfaces do not absorb all incident electromagnetic radiation, but rather reflect some. In order to calculate and analyse radiation for these surfaces, a number of assumptions have to be made. Surfaces are assumed to be isothermal and to be characterised by uniform radiosity and irradiation. Furthermore, the behaviour of the surface is assumed to be opaque, diffuse and gray, whilst the medium surrounding these surfaces is assumed to be non-participating (Incropera & de Witt, 2001).

The net radiative transfer rate from a diffuse, gray surface is then defined as

$$q_i = \frac{E_{bi} - J_i}{\frac{1-\varepsilon_i}{\varepsilon_i A_i}} \tag{3.2}$$

where J is radiosity and E_b is the total emissive power of the surface if it were a blackbody. Based on the definition of the view factor (Section 1.4), the total rate at which radiation reaches surface i from all surfaces, including i, is

$$q_i = \sum_j^N A_i F_{ij} (J_i - J_j) \tag{3.3}$$

where N is the total number of surfaces. Combining Equations (3.2) and (3.3) gives

$$\frac{E_{bi} - J_i}{\frac{1-\varepsilon_i}{\varepsilon_i A_i}} = \sum_j^N A_i F_{ij} (J_i - J_j) \tag{3.4}$$

And the radiative exchange between surfaces is then

$$q_{ij} = \sum_{j}^{N} \frac{(J_i - J_j)}{\frac{1}{A_i F_{ij}}} \tag{3.5}$$

The term $(J_i - J_j)$ is the driving potential of this exchange, whilst $(A_i F_{ij})^{-1}$ is the space resistance. In summary, Equation (3.4) says that the rate of radiation transfer to i through its surface resistance must equal the net rate of radiation transfer from i to all other surfaces through the corresponding space or geometrical resistances (Incropera & de Witt, 2001:806). It is this space resistance, or the view factor, to be precise, that was used to characterise radiation in packed beds in the following sections.

3.2 PROPOSED HYPOTHESIS FOR RADIATION HEAT TRANSFER IN RANDOMLY PACKED BEDS

Attempting to implement the radiation equations in Section 3.1 for each and every pebble surface (in a packed bed) in the heat transfer correlations developed is quite simply impossible. A balance has to be found between simplicity and accuracy.

Thus, in an attempt to simplify the computation of radiation in packed beds, picture the following: - A sphere in the bulk region of a packed pebble bed is under consideration, and named the central sphere. Virtual, concentric and spherical shells surround the central sphere, with the first shell's boundary at the surface of the central sphere, and second shell's boundary at exactly one sphere diameter from the centre of the central sphere. The shells are spaced evenly outwards as seen in Figure 3.1.

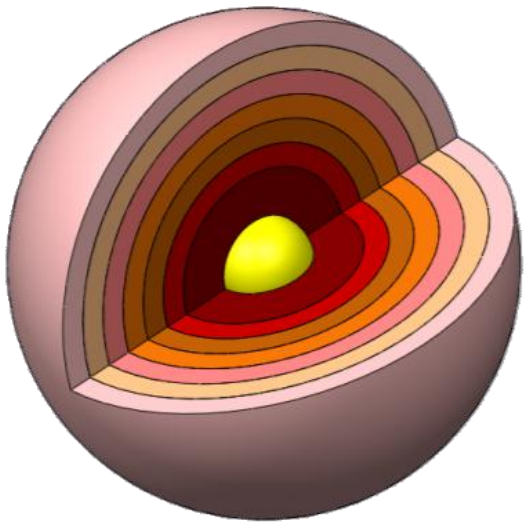

Figure 3.1: Illustration of the shells surrounding a central sphere (van der Meer, 2011).

A hypothesis is proposed that: “Excluding the short range radiation to spheres which are in contact with the central sphere; if the surfaces of all spheres whose centres fall within a spherical shell were assumed to be at a single homogeneous temperature and the view factors and surface areas of all the spheres are added together to represent that of the single shell, the long range radiation to this shell will represent the total long range radiation to all of the individual spheres combined.”

This hypothesis forms the basis of the proposed new Spherical Unit Nodalization (SUN) model.

3.3 METHODOLOGY TO TEST THE HYPOTHESIS

The hypothesis proposed in Section 3.2 simply discretises pebbles surrounding the central sphere into a small number of spherical shells surrounding it. Thus instead of the central sphere radiating to a large number of individual spheres, radiation would be to a limited number of bodies, whose surface temperatures would then represent the temperatures of the individual spheres that they are composed of. This discretisation is necessary, in order not to consider long range radiation as being to a single entity with a single average radiative temperature, such as Van Antwerpen and other authors did. Rather, long range radiation would then be to a number of spherical shells which would be at different radiative temperatures, and would generate better radiative temperature profiles. The numbers of these bodies (thus temperature data points) would be dependent on the fineness of the discretisation.

To test the hypothesis above, a section of the bulk region of a randomly packed bed was drawn in the drawing package Solid Works 2009 (elaborated upon in Section 3.5.1). This test section, now the control volume of the study, was discretised and the bodies of spheres surrounding the central sphere were identified. The test section was then imported into the CFD package Star-CCM+, wherein it was prepared for simulations. View factors from the central spheres to these bodies, which would be difficult to determine theoretically, were calculated using the in-built view factor calculator, and extracted. Simulations on this test section were done purely for the extraction of this data.

Another test section of similar dimensions, in which spheres were not grouped into bodies, but were rather left individualistic as they would be in a packed bed, was also drawn in Solid Works and imported into Star-CCM+. This test section was then prepared for heat transfer simulations. After defining the physics continuity equation models for the simulation, boundary conditions were specified such that the central sphere only radiated heat to all other spheres. The simulation was then solved to determine the surface temperatures of all the other spheres.

Using the view factor data extracted earlier, a separate EES model based on the fundamental radiation heat transfer equations in Section 3.1 and the SUN model approach was developed. This model simulated heat transfer from the central sphere to the spherical shells with homogeneous temperature

and representative view factors surrounding it. The temperature results from the EES model were then compared with the temperature results of the detailed CFD heat transfer simulations. The exact details of the work described above will be elaborated on in Section 3.5 and Chapter 4.

3.4 RADIATION IN STAR-CCM+

The solution of radiation in CFD requires two models, namely a radiative transfer model and a radiation spectrum model. Transfer models define the method of solution for the governing radiation transfer equations. Star-CCM+ has the following transfer models:

- The Surface-to-Surface radiative heat transfer for modelling non-participating media.
- The Participating Media Radiation, also known as the Discrete Ordinates Method (DOM).

The radiation spectrum model defines how the radiation wavelength spectrum is considered and potentially discretised within the context of the transfer model. These spectrum models are:

- Grey Thermal Radiation for modelling wavelength-independent radiation properties.
- Multiband Thermal Radiation for modelling wavelength-dependent radiation properties.

For the Gray Thermal spectrum model, the full thermal wavelength domain is considered as a whole, and all radiative properties are considered invariant within this single spectrum. Whilst for the Multiband Thermal spectrum model, the full-thermal spectrum may be divided into sub-spectra. For each sub-spectrum, waveband-specific properties are defined. During the radiation solution process, the transfer model is applied to each sub-spectrum. The total radiative transfer is the sum of the resulting solutions from the individual sub-spectra.

Surface-to-surface modelling also requires view factors, which are calculated using the view factors calculator within Star-CCM+. The effects of radiation are modelled within the regions in the simulation as well as between the regions. Radiation exchange between the regions takes place whenever the medium or space between the regions is transparent or partially transparent to radiation.

The definition of a radiation problem is completed by defining the properties of the media inside the regions and the surface properties of the boundaries. Non-participating media are transparent to radiation and only require the surface properties of emissivity, reflectivity and transmissivity to be specified on the boundaries. In contrast, participating media may emit, absorb, and scatter radiation and additionally require material absorption and scattering properties to be specified within the regions via the continuum material properties.

One of the inputs for radiation in Star-CCM+ is a variable termed Radiation Temperature under Thermal Environments. This is the temperature at which any rays of radiation which escapes the domain of a simulation to the environment will be radiated to. Depending on the magnitude of the rays and its value, this temperature can have significant effects on simulation results.

3.5 SIMULATION IN STAR-CCM+

3.5.1 Study of View Factors in Packed Beds

Du Toit (2010) developed a numerically packed bed, whose packing was random and recorded the co-ordinates of each sphere. The data was used by the current author to identify a section of the bed in the bulk region to be the area of focus. A sphere at the centre of this region was identified as the central sphere. All other spheres were numbered and through use of their corresponding co-ordinates, their distances from the central sphere were calculated. This test section, as shown in Figure 3.2, was then drawn in Solid Works to generate simple surface boundaries for Star-CCM+. The spheres from the numerically packed bed were 60 mm in diameter, and this was based on the fact that the PBMR intended using pebbles of that size. When preparing the test section in Solid Works, however, the spheres were made exactly 59 mm in diameter, whilst their co-ordinates were unchanged. This is because:

1. In the heat transfer simulations that are to follow, heat conduction in between solids has to be avoided, as the focus is on thermal radiation. Thus no solids should be in contact.
2. An interface has to be defined for any region which is in contact with any other region in Star-CCM+. For a randomly arranged domain such as for the test section, this would have been a mammoth task.

For all post-processing of data, however, the spheres were taken to be 60 mm in diameter to eliminate confusion. Initially a square shaped control volume was used, as the optimal shape for the hypothesis was not known yet. The test section was 420 x 420 x 420 mm^3, which is $7d \times 7d \times 7d$ in sphere diameters. As no heat transfer simulation was to be performed yet, the physics continua and the fluid medium were not defined.

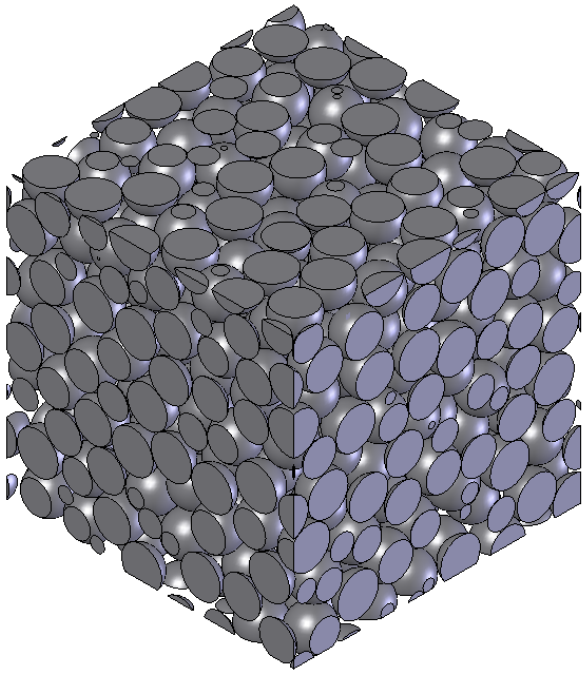

Figure 3.2: The test section of a randomly packed bed drawn in Solid Works.

The simple surface boundary was then imported into Star-CCM+, where new surface and volume meshes would be generated for the spheres, which are now regions in Star CCM+. A polyhedral mesh with a base size of 15 mm (explained later in Section 3.5.2.2) was selected for the mesh type because of its ability to adapt to varying geometry of regions.

Figure 3.3: Face view of the polyhedral volume mesh.

The first investigation conducted was to determine the view factors from the central sphere to all other spheres surrounding it. Star-CCM+'s in-built view factor calculator was used to generate the view

factors, which were then extracted to MS Excel for further processing. The results are shown in Figure 3.4. The results presented in the figure will be discussed below.

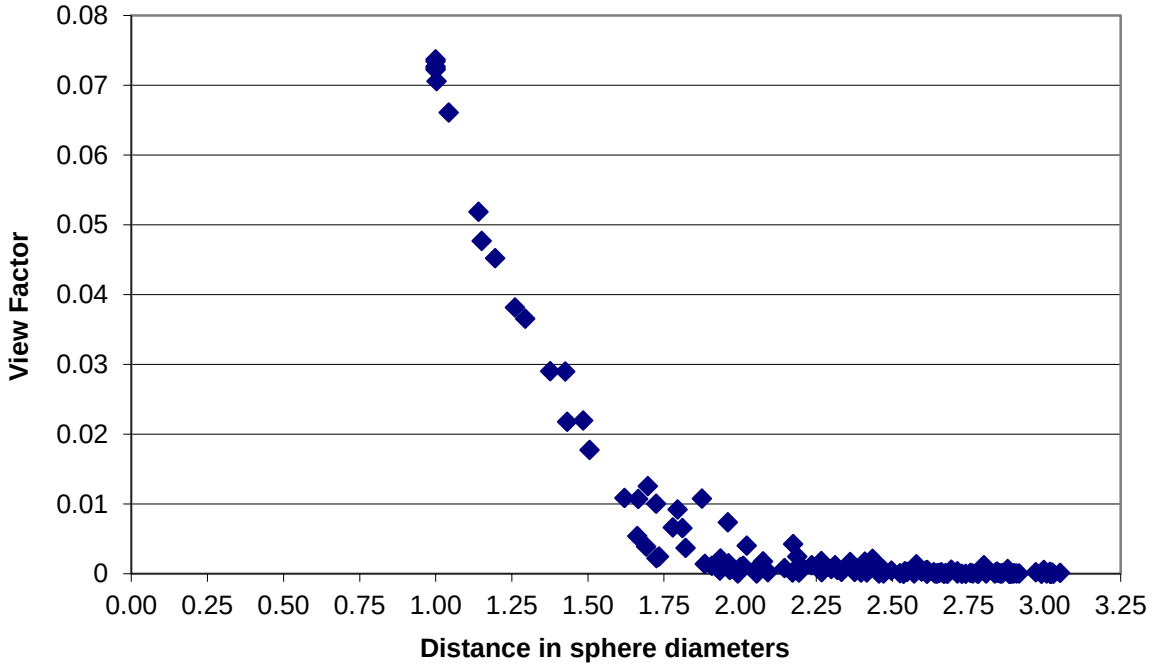

Figure 3.4: View factors in the bulk region of a randomly packed bed.

Wakao and Kato (1968) found that the diffuse view factor for two half spheres that are in contact is equal to 0.1511. This view factor was based on half of the surface area of a sphere. For a view factor based on a full sphere surface (which will be our reference surface area throughout), it would be

$$F_{12} = 0.07555 \tag{4.1}$$

Based on the rule of reciprocity that $A_i F_{ij} = A_j F_{ji}$. This view factor and the results of Star-CCM+ (average view factor to all spheres in contact with central sphere) are compared in Table 3.1 below:

Table 3.1 Comparison of short range view factor.

Wakao & Kato	Star-CCM+	Difference	% Difference
0.07555	0.07160	0.00395	5.52%

With a percentage difference of only 5.52 %, the results provided by the view factor calculator within Star-CCM+ is accepted as sufficiently accurate and will be relied upon to determine view factors between other surfaces.

Reverting back to Figure 3.4, the maximum view factor is at one sphere diameter, as is to be expected since this is for spheres that are in direct contact with the central sphere. From there the view factors

decrease exponentially, and start to approach zero at two sphere diameters away. It can be deduced that a sphere in the bulk region of a randomly packed bed has no view of other spheres whose centre points are at a distance of 2.25 sphere diameters or more away from its centre point.

The second investigation undertaken was to determine how the view factor from the spheres to the wall decreased in the near wall region, seeing as the porosity of the packing would differ from that of the bulk region. Once again, data from the numerically packed bed was used to identify a section at the outer near wall region. This section was drawn in Solid Works to generate the surface boundaries for Star-CCM+. A slightly concave wall, which represented the side reflector, was added. A 2 mm gap was kept between wall and the sphere so that no solids are in contact. The test section, in Figure 3.5, was 420 x 420 x 280 mm^3, which is $7d \times 7d \times 4d$ in spheres diameter. In a similar manner to the earlier investigation, the test section was imported into Star-CCM+ and the view factors were determined.

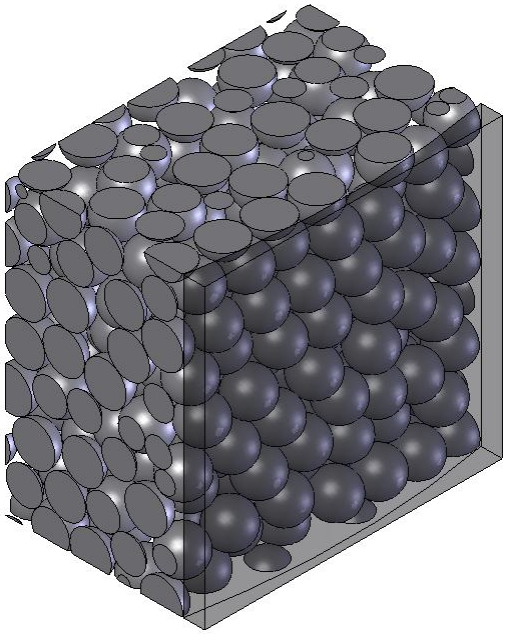

Figure 3.5: The wall for this near wall test section was made transparent for visual purposes.

It has already been establish that the view factor is zero at $2.25d$ from a sphere. Thus only the results of the spheres at the centre of the test section were considered. i.e. spheres within the inner rectangular core of $2.5d \times 2.5d \times 4d$. This is to eliminate the effects of the environment (space surrounding the test section, or control volume within Star-CCM+) on the results. The results from this investigation are shown in Figure 3.6 below.

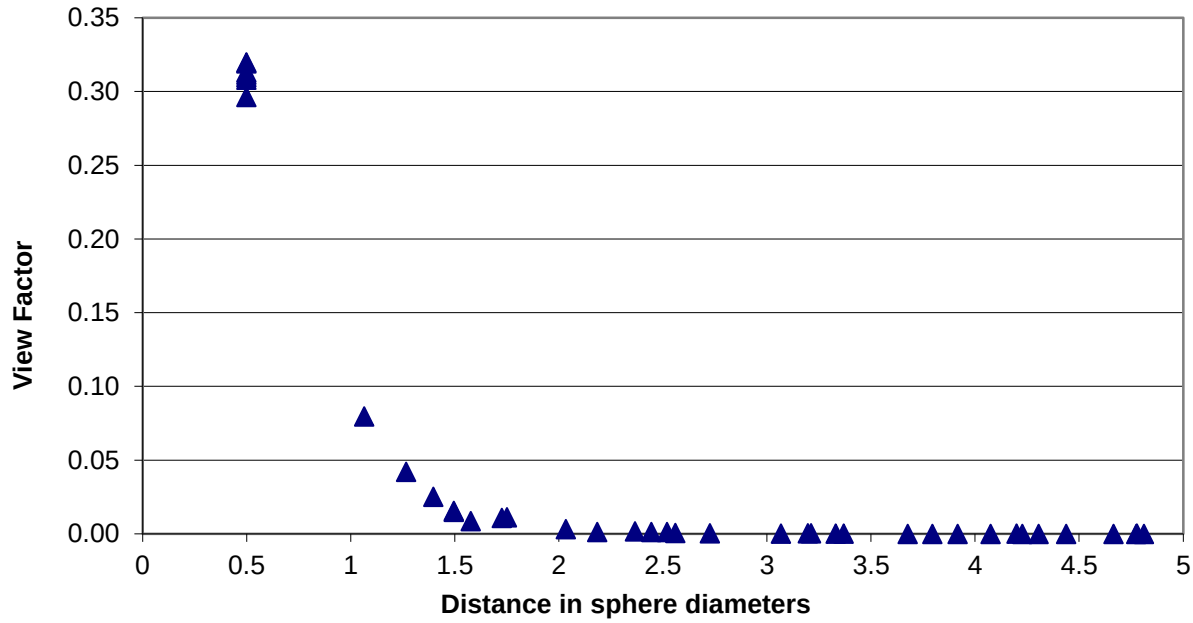

Figure 3.6: View factors from spheres to the reflector at the near wall region.

The spheres closest to the wall, which were at a distance of $0.5d$ to the wall, had an average view factor of $F_{12} = 0.31100$ to the wall. The view factors from other spheres then decreased exponentially, approaching zero at a distance of $2d$.

For the purposes of comparison, the investigation was extended to another packing structure. A simple structured cubic packing of spheres shown in Figure 3.7 was prepared and view factors, whose results are shown in Figure 3.8, were determined.

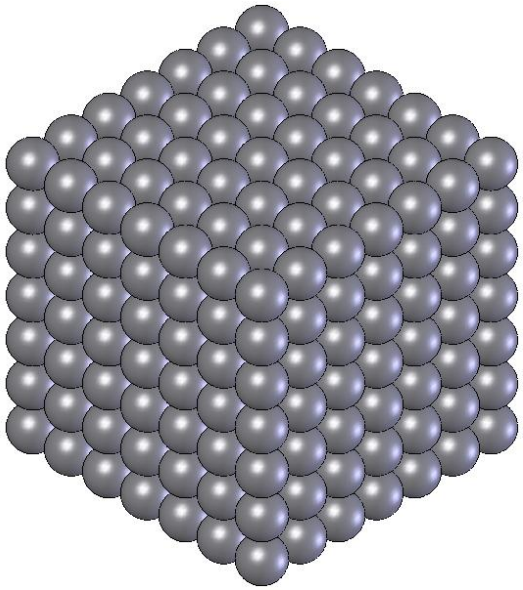

Figure 3.7: A simple cubic packing structure.

Typically, with a simple cubic packing structure, a number of spheres would be equidistant from the central sphere. Thus in Figure 3.8, although it might look like it, it doesn't mean that there are fewer data points. It is the nature of the structure that those equidistant spheres would be similarly shaded from the central sphere, and thus would have similar view factors.

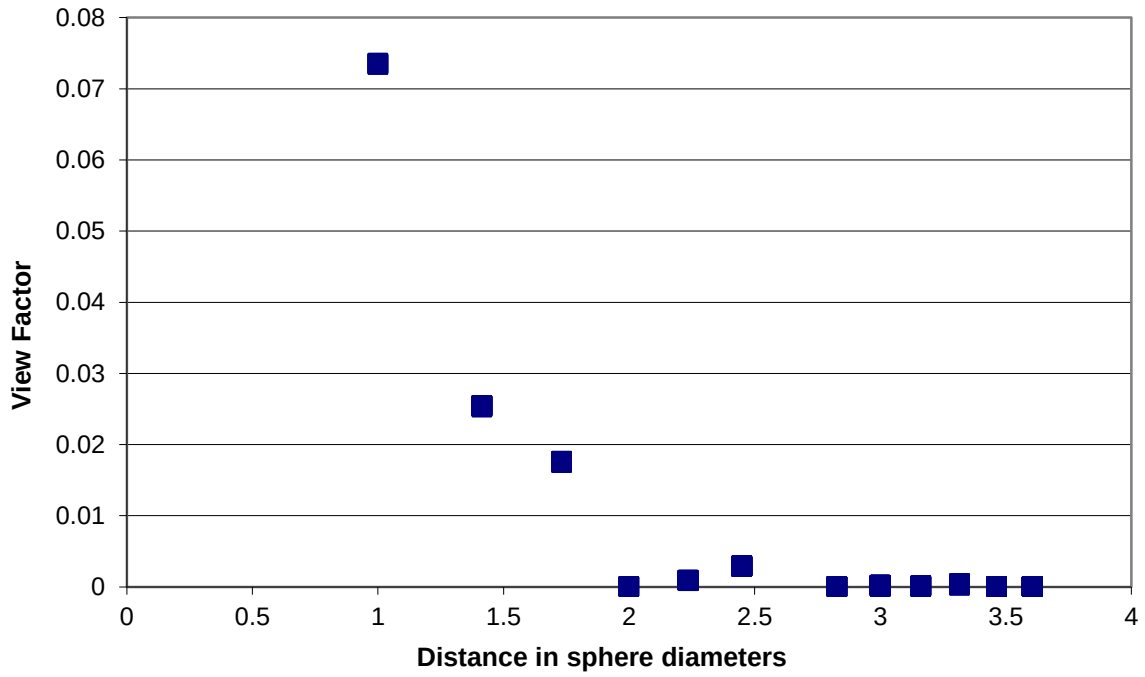

Figure 3.8: View factors in the bulk region of a bed with simple cubic packing structure.

The average short range view factor for the simple cubic packing is $F_{12} = 0.07347$. It is within only 2.83% from the theoretical value in Equation (4.1). It then drops very sharply, once again approaching zero beyond a distance of $2.25d$. The zero view factor at $2d$ is simply because those spheres have other spheres directly blocking their view from the central spheres, and are thus completely hidden.

The above investigations have revealed that in packed beds, the view factor from a central sphere approaches zero from $2d$ and is almost completely zero by $2.25d$. The shape of the decrease in the view factor also supports the notion that spheres in the long range radiation region cannot simply be grouped as one single surface. If the net radiative exchange cannot be determined for each individual sphere, then the long range radiation spheres should be divided or discretised into a number of groups. The long range group closest to the central sphere would then have a larger view factor, which implies a higher radiative temperature than the rest of the groups, which in turn should give better temperature profiles.

3.5.2 The Model for Heat Transfer Simulation

To test the hypothesis that led to the Spherical Unit Nodalization model proposed in Section 3.2, radiation heat transfer data was needed to compare against. A test section detailed below was thus prepared for simulation in Star-CCM+.

3.5.2.1 Selection of the Geometry for the Control Volume

The hypothesis is based on having concentric spherical shells around the central sphere, thus the test section for the heat transfer simulation was spherical. The test section in Figure 3.2 was re-drawn to be spherical, but the co-ordinates of the spheres were maintained. It should be noted that although a randomly packed bed was used, the hypothesis should just as well apply to any other packing structure.

It has already been established that a central sphere has no view of other spheres at a distance further than $2.25d$ from it, thus this test section should have a minimum diameter of $4.5d$ from the centre of the central sphere. To ensure a margin of safety, and a more realistic representation of a packed bed, whilst keeping the test section small enough for the computing capacity available, the diameter of the test section was doubled to $9d$ (540 mm). Thus if the spheres were to form a straight line thorough the centre, there would be four spheres on each side of the central sphere. The cross section of the test section for the simulation after preparation for simulation in Star-CCM+ is shown in Figure 3.9 below.

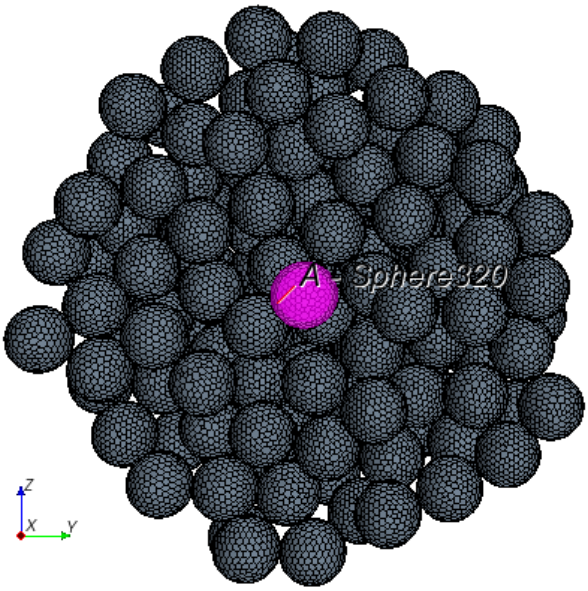

Figure 3.9: Volume mesh wrapped spheres with the central sphere highlighted.

3.5.2.2 The Physics for the Simulation

The primary interest for the simulation is radiation heat exchange from the central sphere to other spheres and the exchange amongst other spheres. Thus the other modes of heat transfer, conduction and convection, had to be eliminated.

Conduction in-between the spheres was eliminated through the gap that was maintained in-between all spheres within the test section. To ensure that the thermal conductivity of the solid material's did not influence the results significantly, it was fixed at a very high value of $k_s = 10000\ W/m-K$. Thus any heat radiation that is incident on one side of a sphere would be directly conducted to all surfaces.

Convection was eliminated by having no fluid medium in-between the spheres. As the Surface-to-Surface radiative heat transfer model was used, there was no need to specify a fluid medium. This is a great benefit as specification of a medium would have required definitions of all interfaces between the medium and the solids.

This non-interest in the conduction through the solids and the lack of convection allowed for use of a 'coarser' grade of meshing than typical. Hence the use of a base size of 15 mm on spheres whose diameters are 59 mm. Polyhedral meshing, which can adapt to smaller sizes where necessary, was selected and prim layers which ensure consistent expansion and contraction of the mesh were utilised.

Full enclosure of the simulation domain was achieved through covering the test section with a 5 mm thick solid 'ball' with an outer diameter of 560 mm. There was thus a 5 mm gap between the inner surface of this cover and the outer most spheres of the test section, to ensure no conduction of heat to the cover. This cover ensured that no heat radiation from the spheres could escape the domain to the environment, where the Star CCM+ input radiation temperature would influence the results.

Furthermore, the behaviour of the surface is assumed to be opaque, diffuse and gray. The emissivity of all solids was fixed at $\varepsilon = 0.8$ (the default value for graphite in Star-CCM+). The emissivity at the external surface of the cover was, however, specified to be $\varepsilon = 0.0$, once again to ensure that there is no radiation to the environment.

A temperature boundary condition of $T = 1189°C$ was specified at the surface of the central sphere, whilst a heat flux of $Q = 1946.8462\ W$ which exited the domain was specified at the external surface of the cover. The initial boundary conditions were set at $T = 1200°C$ for the central sphere, and $T = 590°C$ for all other solids. These values are sufficiently far enough from the expected final results, but close enough as well so as not to cost precious computational time.

Having defined all physics continua and the boundary conditions, the simulation was set to solve to a point where steady state is achieved.

4. Results

4.1 CONVERGENCE TEST FOR THE RESULTS

There is no absolutely definitive test for convergence for any numerical solution and numerical solutions by their nature contain errors. The goal is to keep those errors at a minimum and acceptable level. The following methods were used to check the error of the simulation.

4.1.1 Residuals

In the simulation, only heat transfer was being simulated, thus the differential equation being solved was an energy equation. The residuals from the simulation are indicated in Figure 4.1 below. In Star CCM+, a residual within a cell is defined as the degree to which a discretised equation is not completely satisfied, thus the residual represent the absolute error. Ideally, for a perfectly converged solution, the round off of the residuals as in Figure 4.1 would equal the residual for each cell.

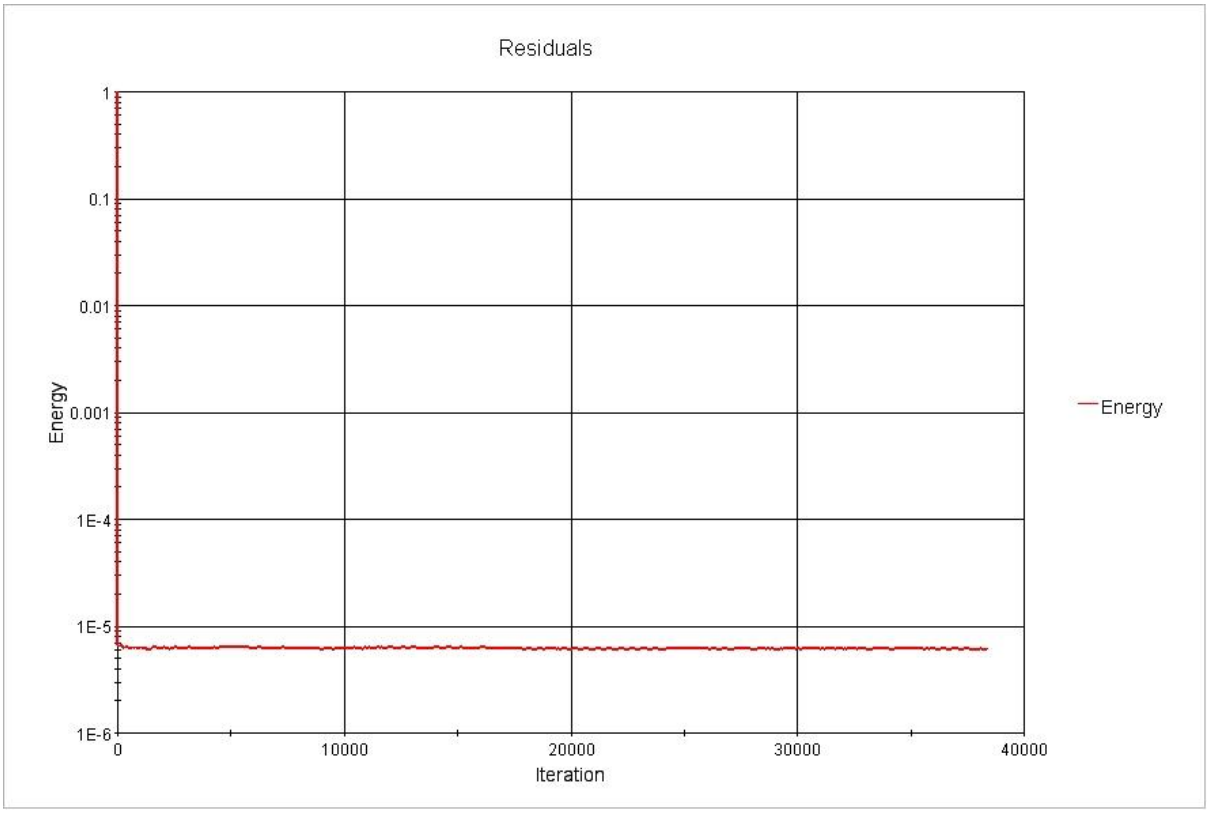

Figure 4.1: Residuals of the heat transfer simulation.

A general rule of thumb is that the residual should be in the order of 3-5 orders of magnitudes less than the initial residual. The error in the graph below dropped sharply in the first 100 iterations or so, reaching the order of 5 magnitudes whilst the solution was still far from the expected temperatures. It then stayed constant whilst the temperatures approached their expected values. At the last iteration,

no. 38400, the energy error was 6.037 E-06. This shape of the graph could not be immediately explained, but it could be due to the non-linearity of the radiation equations.

4.1.2 Heat Flux and Radiosity

The heat extracted from the domain at the external surface of the cover is $Q = 1946.8462W$. Since no other heat is generated or absorbed by the other pebbles, the same amount of heat should be generated by the central sphere. This central sphere, with a diameter of $d = 0.059m$, has an area of $A = 1.09359E-02\,m^2$. Thus the heat flux through the surface should be $\dot{Q} = 1.78023\text{E}05W/m^2$ on average. The results from the simulation are shown in Figure 4.2 (Values are negative as radiation is from the central sphere). Star-CCM+ currently presents its results visually only, and there is no results file. Thus it is not easy to determine the exact percentage differences.

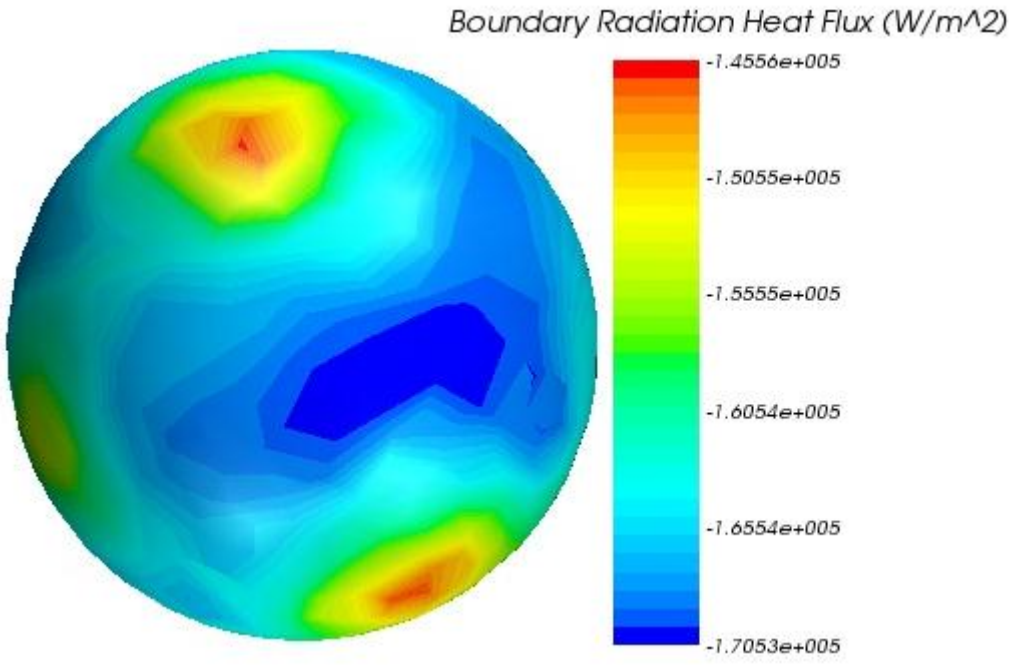

Figure 4.2: Heat flux distribution around the central sphere.

Phrased another way, the expected radiosity from the central sphere was calculated to be $J = 2.15628\text{E}05W/m^2$. The simulation results are shown in Figure 4.3 below. The values for both heat flux and the radiosity from the simulation are in the range of the numbers that were expected.

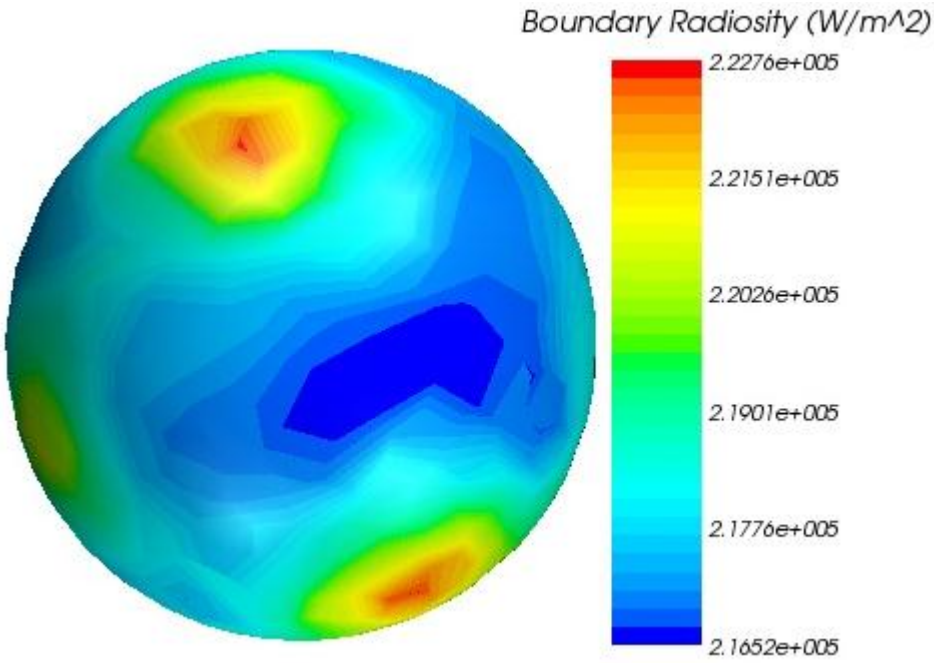

Figure 4.3 Radiosity from the central sphere.

4.1.3 Monitor Points

One of ways to monitor a simulation is to track the value of a specific variable at a particular location. This will typically be areas where flow is slowest, or a variable which is most dependent on other variables. As only temperatures were solved for in this simulation, it was not easy to pin-point such an area. The temperature of the external surface of the cover was selected as it is the lowest temperature and also the furthest temperature from the central sphere, where a temperature boundary condition was specified. The decrease in this temperature is tabled in Table 4.1. From 30,000 to 38,400 iterations, the cover temperature dropped by only 2.63 °C. Whilst the drop in temperature might be small, it had cost dearly in terms of computational time. Figure 4.10 shows this cover surface temperature at the last iteration.

Table 4.1 Cover temperature as tracked per iterations.

Item	Iteration	Cover Temperature [°C]
1	1	490.00
2	500	489.21
3	1000	488.39
4	10000	476.77
5	15000	472.01
6	20000	468.22
7	25000	465.27
8	30000	462.97
9	35000	461.18
10	38400	460.34

Based on the results of the above three monitoring methods, it was accepted that the simulation has reached steady state, and the simulation was stopped after 38,400 iterations.

4.2 VALIDATION OF RESULTS

An EES model of the Spherical Unit Nodalization model was developed to compare to the CFD results. Using the test section in Figure 3.2, the spheres around the central sphere were discretised and grouped into shells of bodies, named R1, R2… R7 and R8 represented the external environment or the cover. The geometry of these shells are detailed in Table 4.2 where the boundaries and the radii of the shells are given in terms of sphere diameters. The exact number of spheres within the R7 shell could not be determined, as some of the spheres were cut when drawing the test section.

Table 4.2: Geometry of SUN model shells.

Shell	Boundaries	Radius of Shell	No. of Spheres Included	Area of the Spheres
Units	d	d		m^2
R 1	$r = 0$	0.00	1	$1.0936\mathrm{E}-02$
R 2	$r = 1$	1.00	7	$7.6551\mathrm{E}-02$
R 3	$1 < r \leq 1.5$	1.25	9	$9.8423\mathrm{E}-02$
R 4	$1.5 < r \leq 2$	1.75	24	$2.6246\mathrm{E}-01$
R 5	$2 < r \leq 2.5$	2.25	36	$3.9369\mathrm{E}-01$
R 6	$2.5 < r \leq 3$	2.75	52	$5.6867\mathrm{E}-01$
R 7	$3 < r < 4.5$	3.75		3.6247
R 8	$r = 4.5$	4.50	Cover / Environment	

The test section which now had the shells defined was then imported into Star-CCM+, the aim of which was to determine the view factors in-between the shells. The results of this calculation are shown in Table 4.3.

Table 4.3: View factors in-between the shells.

	F(1,j)	F(2,j)	F(3,j)	F(4,j)	F(5,j)	F(6,j)	F(7,j)
R 1	0	0.072060	0.035880	0.005431	0.000931	0.000201	1.250E-05
R 2	0.501000	0.171400	0.181800	0.104100	0.022110	0.004510	0.000308
R 3	0.320700	0.233800	0.157600	0.097160	0.068300	0.010220	0.000653
R 4	0.129400	0.357000	0.259000	0.217900	0.171100	0.103300	0.005960
R 5	0.034200	0.116900	0.280800	0.263900	0.206500	0.175600	0.030340
R 6	0.010580	0.034070	0.060050	0.227800	0.251000	0.192700	0.076810
R 7	0.004042	0.014360	0.023660	0.081030	0.267500	0.473700	0.623100
R 8	0.000121	0.000519	0.001115	0.002639	0.012530	0.039730	0.262800

Data from Table 4.3 and the radiation equations in Section 3.1 were then programmed into EES to formulate the SUN model. The view factors from R8 to the other shells were determined using the reciprocity rule within the EES model. Values such as the emissivity and the boundary conditions, i.e. the surface temperature of the central sphere and the heat extracted from the outer shell, were kept the same as in the CFD simulation. Further details of this EES model can be found in Appendix A. The

average surface temperatures of these shells were then calculated, the results of which are presented in Section 4.4.

4.3 ACTUAL CFD SIMULATION RESULTS

Figure 4.4 shows a cut through the centre of the test section with the simulation results. The central sphere shown in red has its temperature fixed at 1189 °C.

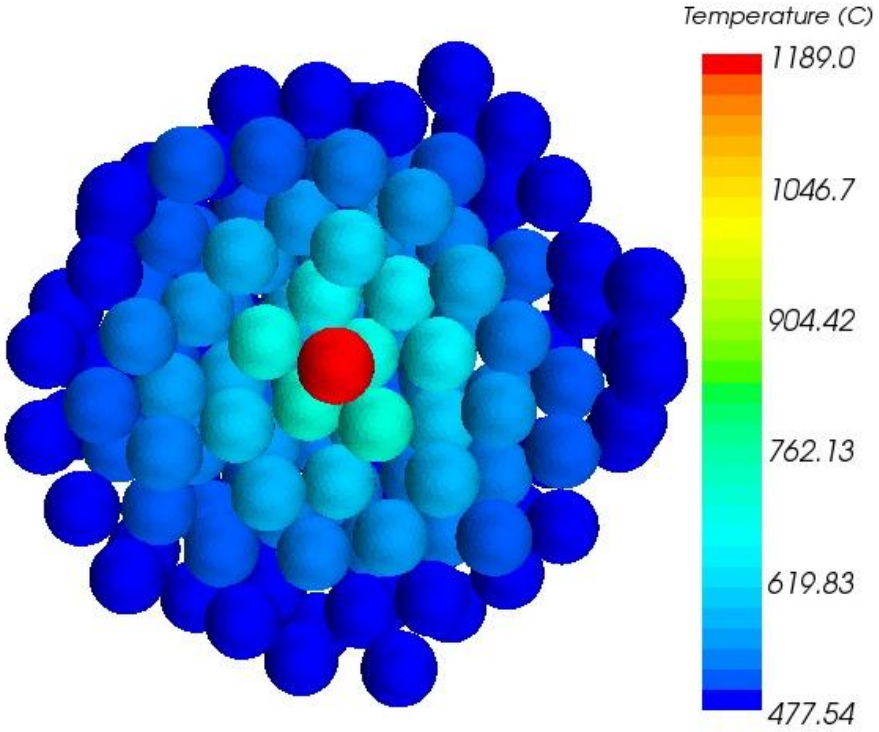

Figure 4.4: Temperature results of the CFD simulation.

Other spheres' temperature results are shown in the next figures per shells within which they lie.

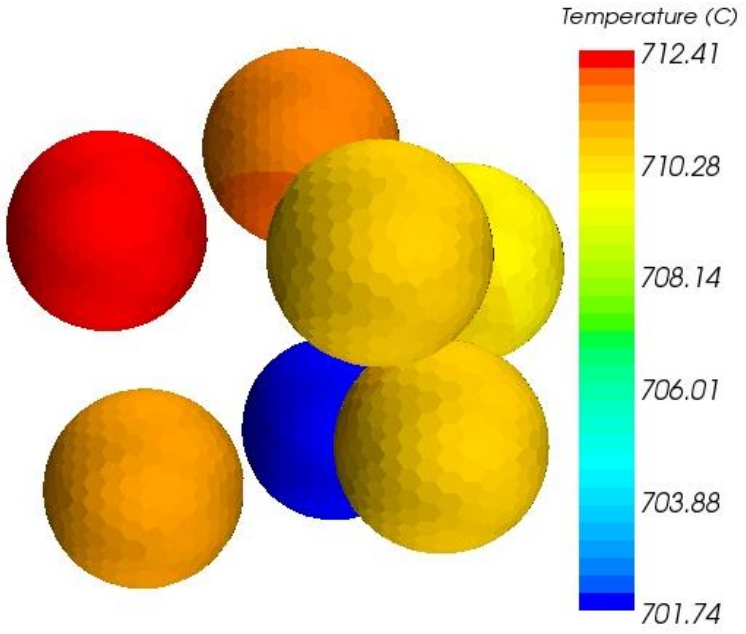

Figure 4.5: Temperatures of the short-range spheres, R2.

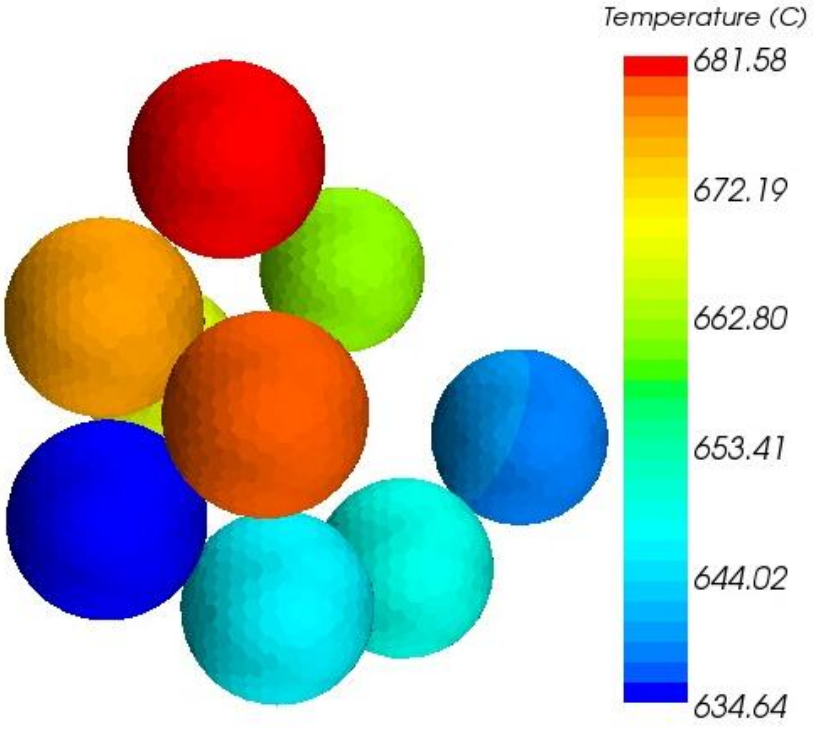

Figure 4.6: Temperatures for spheres within R3.

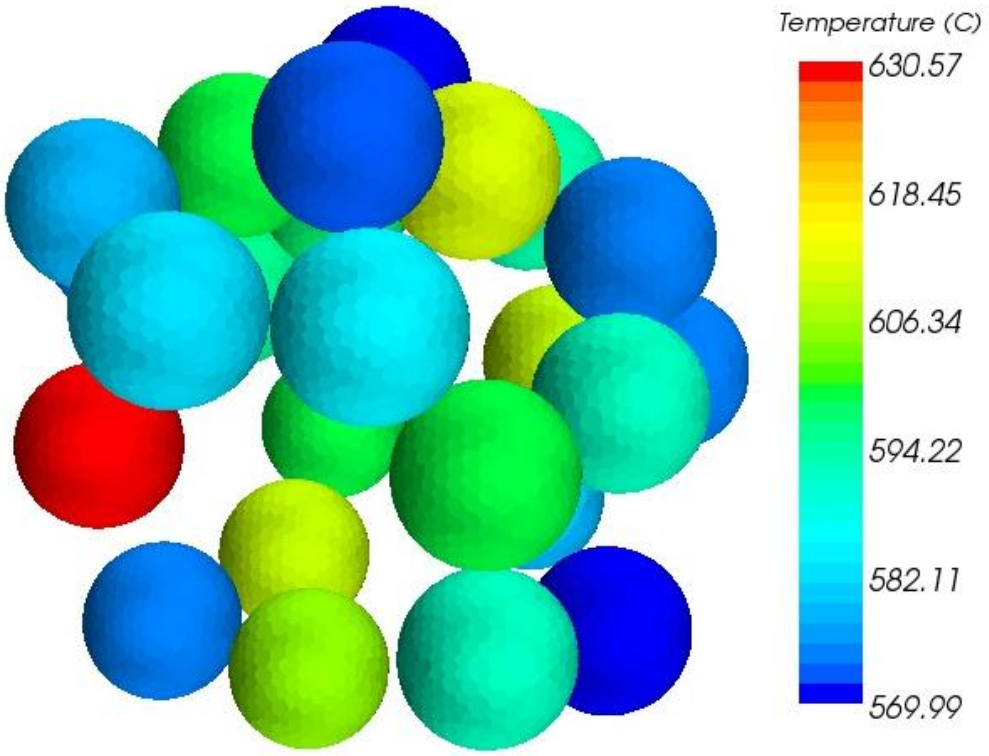

Figure 4.7: Temperatures for spheres within R4.

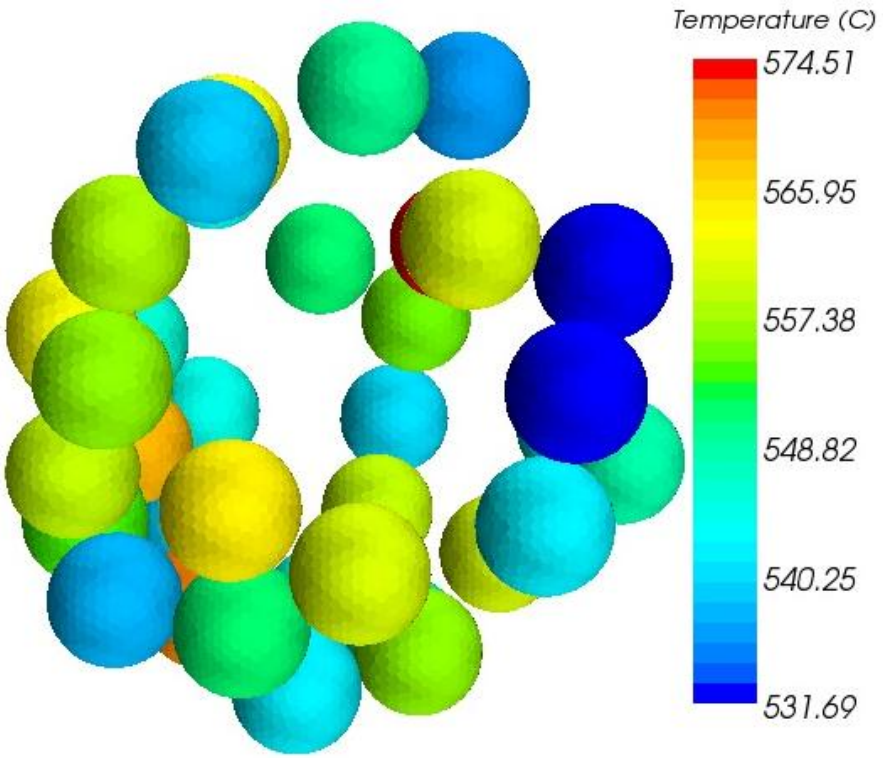

Figure 4.8: Temperatures of spheres within R5.

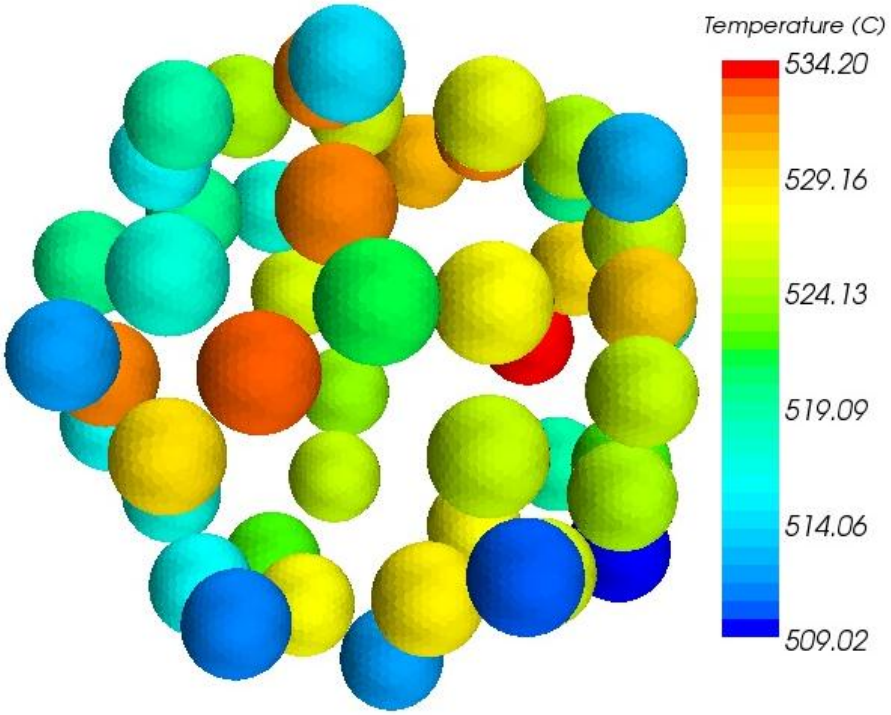

Figure 4.9: Temperatures for spheres within R6.

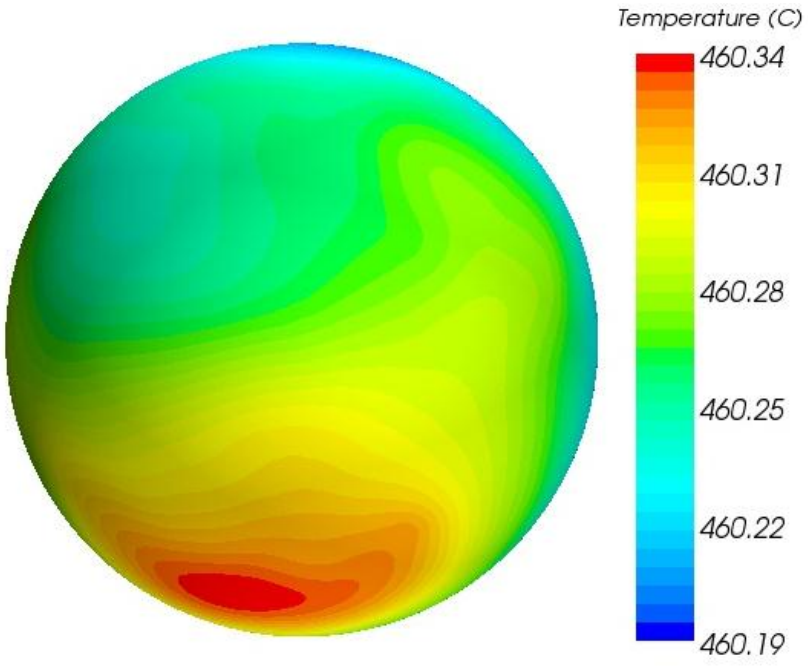

Figure 4.10: The cover's surface temperature.

Since the results from Star-CCM+ are displayed only visually, the surface temperatures of each sphere had to be extracted manually into MS Excel. Because the solid thermal conductivities of the spheres were deliberately set at a very high value, the temperature across the surface of each sphere was in essence constant, with the maximum difference in temperature across a sphere being 0.27 °C.

Nonetheless both the minimum and maximum temperatures were noted, and the surface temperature was averaged between the two.

Figure 4.11 shows at the temperature profile of the CFD simulation as a function of the distance from the central sphere, with the central sphere's temperature not indicated.

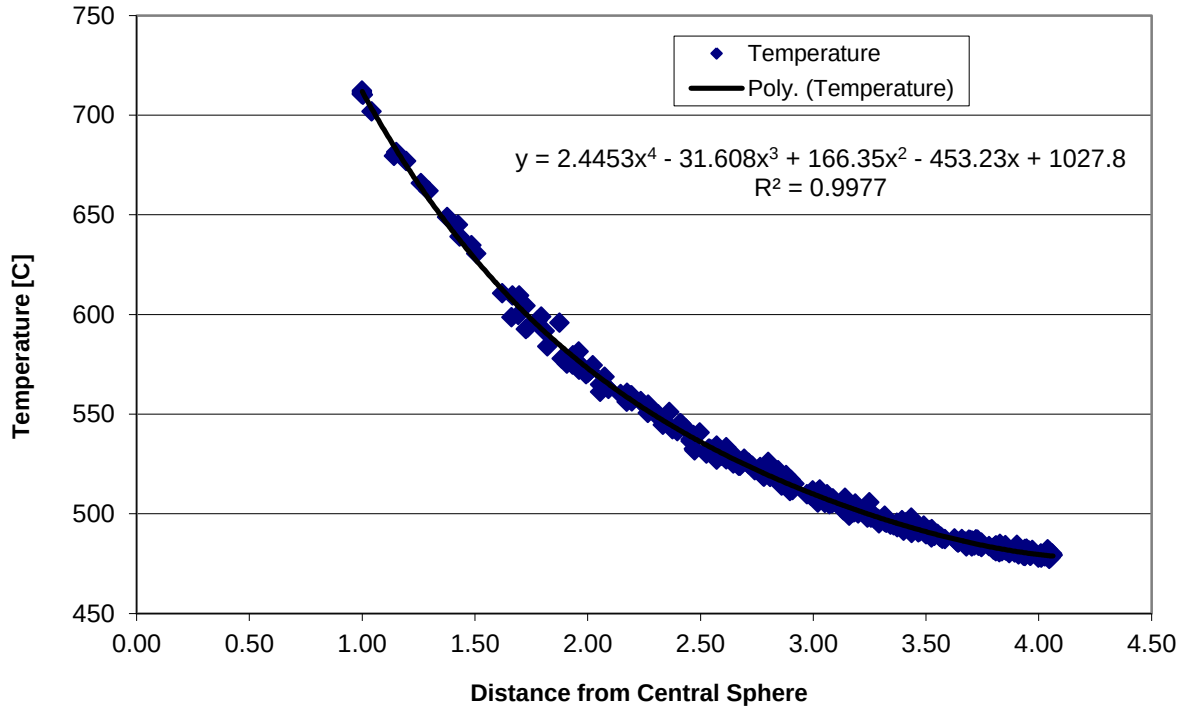

Figure 4.11: Temperature profile of the randomly packed bed.

4.4 COMPARISON

Results from the CFD simulation are presented as per average surface temperature of all spheres within a shell, although the spheres were, however, simulated individually. In the first case of comparison, the boundary conditions of the SUN model were fixed to be exactly the same as the boundary conditions of the CFD simulation, which were $T = 1189°C$ at the central sphere and a heat flux of $Q = 1946.8462W$ at the external surface of the cover. Results of this case are shown in Table 4.4 below.

Table 4.4: Comparison of the CFD and SUNs model results with the same boundary conditions.

Distance	Shell	CFD	SUN	Difference	% Difference
d		°C	°C	°C	
0.00	R 1	1189.00	1189.00	0.00	0.00%
1.00	R 2	709.80	684.54	25.26	3.69%
1.25	R 3	659.26	639.94	19.32	3.02%
1.75	R 4	590.35	580.03	10.32	1.78%

Distance	Shell	CFD	SUN	Difference	% Difference
2.25	R 5	551.35	545.92	5.43	0.99%
2.75	R 6	522.32	521.65	0.67	0.13%
3.75	R 7	490.35	494.21	-3.86	-0.78%
4.50	R 8	460.34	470.02	-9.68	-2.06%

In the second case of comparison, the temperatures of the shells R1 and R8 within the SUN model were fixed to be similar to the CFD simulation results. i.e. $T = 1189°C$ at the central sphere and $T = 460.34°C$ at the cover. The aim was to check the heat flux that would be calculated by the SUN model, the results of which are in Table 4.5.

Table 4.5: Heat flux as determined by the SUN model using CFD results.

CFD	SUN	Difference	% Difference
W	W	W	
1946.8462	1953.9	-7.0538	-0.36%

The second comparison also produced temperatures profiles, which are compared in the following Table 4.6 .

Table 4.6: Temperature profiles of the SUN model for the second comparison.

Distance	Shell	CFD	SUN	Difference	% Difference
d		C	C	C	
0.00	R 1	1189.00	1189.00	0.00	0.00%
1.00	R 2	709.80	680.64	29.16	4.28%
1.25	R 3	659.26	635.26	24.00	3.78%
1.75	R 4	590.35	574.02	16.33	2.84%
2.25	R 5	551.35	538.99	12.36	2.29%
2.75	R 6	522.32	513.96	8.36	1.63%
3.75	R 7	490.35	485.53	4.82	0.99%
4.50	R 8	460.34	460.34	0.00	0.00%

The results between the SUN model and CFD simulations compare well. In the first comparison, the maximum percentage difference is 3.69%, which is acceptable for the simplification that the SUN model brings forth. In nominal terms, the largest temperature difference is at the short range spheres (R2), which is 25.26 °C. In Table 3.1, it was shown that short range view factor calculated by Star-CCM+ is slightly different from the theoretical value. This is probably due to the 2 mm gap that is maintained between spheres to avoid conduction. In the theoretical case, the spheres are in contact with one another. This slight error might manifest itself in temperatures, and as radiation temperature calculations are to the power of 4, this error would be magnified. Further from the central sphere, these gaps are of less significance. The SUN model's temperatures matched the average surface temperature of the spheres to within 12 °C.

The heat flux calculated by the SUN model in the second comparison is 1953.9 W, which differs by 0.36 % to the heat flux used for the CFD. The temperature of the cover from the CFD results, which was entered into the SUN model for the second comparison, is 10 °C lower than the temperature calculated by the model for the first comparison. Thus the differences between the SUN model and the CFD results in the second comparison are greater, especially at short range. Percentage-wise, these differences are small and within 5 %. But the significant nominal differences at short range could be investigated further in subsequent studies.

The temperatures results for the first comparison are compared graphically in Figure 4.12.

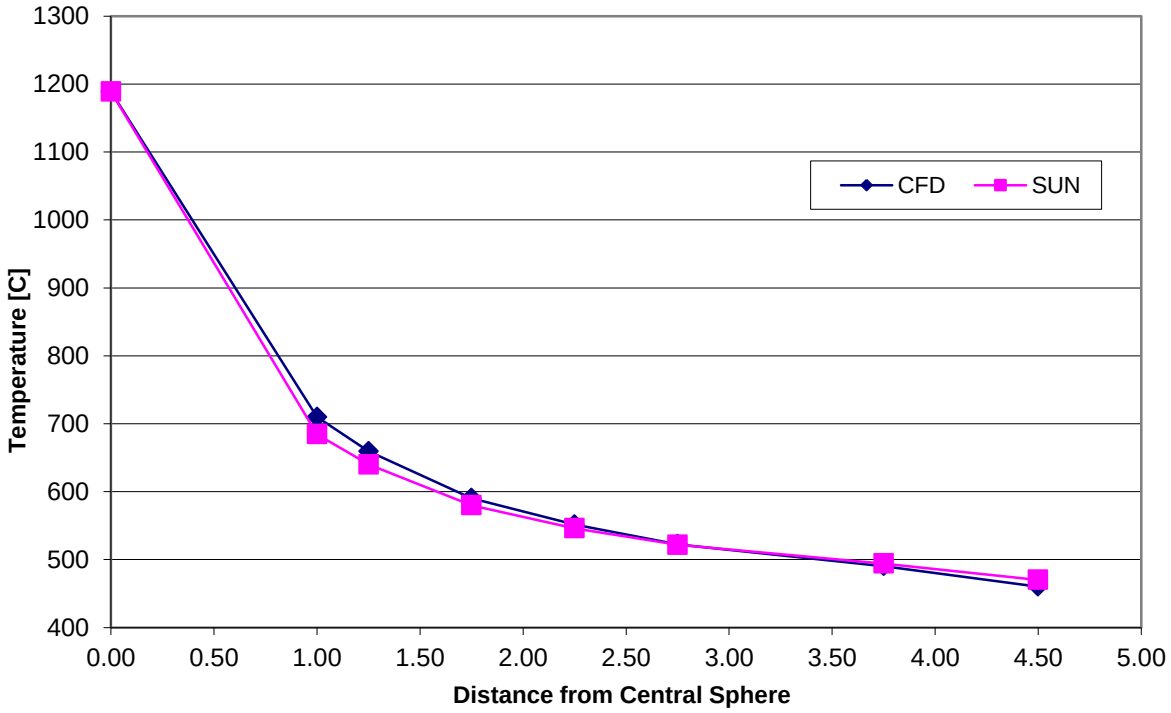

Figure 4.12: Graphical comparison between CFD and the SUN model's results.

5. Summary and Conclusions

5.1 SUMMARY

With the study, the first goal was to study thermal radiation in a packed bed of spheres and characterise the long range radiation component. This was achieved through extensive use of Star-CCM+ to determine view factors in packed pebble beds. The following were established:

1. The distribution of view factors from a central sphere to others in the bulk region of two packings, namely random and simple structured cubic.
2. The distribution of the view factors from spheres in the near wall region to the reflector.
3. The view factor from a sphere closest to the wall, to the wall itself was determined, and found to be on average $F_{12} = 0.31100$.
4. It was determined that in the two packings studied, a sphere has no view of spheres that are $2.25d$ or further away from it. Thus there will be no direct radiation to a sphere beyond this distance.
5. Data on view factors and surface areas within packed beds is now available, and may be used for further studies.

The second goal was to test the hypothesis on how to calculate long range radiation in a simplified manner. This hypothesis led to the Spherical Unit Nodalization Model. To test it, a radiative heat transfer simulation was performed with the help of Star-CCM+. The results of the SUN model compared well with the CFD simulation, thereby proving the hypothesis to be valid.

5.2 CONCLUSIONS

Based on the findings elaborated on above, the aims of this study have been achieved. The new quantitative results is valuable since it can be of use to other researchers in the field of packed pebble beds. Another major finding is the validation of the hypothesis - that radiation heat transfer can be discretised into smaller, manageable segments with homogeneous temperatures. The newly developed SUN model can be expanded on and made use of to predict sphere temperatures due to radiative heat exchange. The model is conceptually simple and computationally efficient, whilst managing to predict the temperatures and heat flux with sufficient accuracy.

5.3 RECOMMENDATIONS FOR FURTHER RESEARCH

The SUN model was developed for a spherical unit cell in the bulk region of a randomly packed bed. The following are some of the suggestions emanating from its development, as to develop it further:

- Transform the SUN model for use in cylindrical co-ordinates, as typical PBRs would have cylindrical or annular cores.
- Following which the radial component should be extracted, as effective thermal conductivity is in the radial direction.
- The SUN model can be tested for other packing structures.
- The results of the SUN model and the CFD simulations can be further improved upon. By, e.g., increasing the size of the spheres to closer to 60 mm, whilst maintain a smaller gap between spheres.

References

ABOU-SENA, A., YING, A. & ABDOU, M., 2007. Experimental measurements of the effective thermal conductivity of a lithium titanate (Li_2TiO_3) pebbles-packed bed, *Journal of Materials Processing Technology*, 181(3):206-212.

AICHLMAYR, H.T. & KULACKI, F.A., 2006. The effective thermal conductivity of saturated porous media, *Advances in Heat Transfer*, 39: 377-460.

BAHRAMI, M., YOVANOVICH, M.M. & CULHAM, J.R., 2006. Effective thermal conductivity of rough spherical packed beds, *International Journal of Heat and Mass Transfer*, 49:3691-3701.

BALAKRISHNAN, A.R. & PEI, D.C.T., 1979. Heat Transfer in Gas-Solid Packed Bed Systems 2. The Conduction Mode, *Industrial & Engineering Chemistry Design & Development*, 18(1):40-46.

BREITBACH, G. & BARTHELS, H., 1980. The radiant heat transfer in the high temperature reactor core after failure of the afterheat removal systems, *Nuclear Technology*, 49(3):392-399.

CHEN, J.C. & CHURCHILL, S.W., 1979. Radiant heat transfer in pebble beds, *American Institute of Chemical Engineers*, 9(1):35-41.

DU TOIT, C.G., ROUSSEAU, P.G., GREYVENSTEIN, G.P., & LANDMAN, W.A., 2006. A systems CFD model of a packed bed high temperature gas-cooled nuclear reactor, *International Journal of Thermal Sciences*, 45:70-85.

DU TOIT, C.G., 2010. Private Communication.

INCROPERA, F.P. & DE WITT, D.P., 2001. Fundamentals of heat and mass transfer, 5th Ed. John Wiley & Sons.

KOSTER, A., MATZNER, H.D. & NICHOLSI, D.R., 2003. PBMR design for future, *Nuclear Engineering and Design*, 222(2-3):231-245.

LAMARSH, J.R. & BARATTA, A.J., 2003. Introduction to Nuclear Engineering, 3rd Ed. Prentice Hall.

NICHOLLS, D.R., 2000. Status of the pebble bed modular reactor, *Nuclear Energy*, 39(4):231-236.

PRASAD, V., KLADIAS, N., BANDYOPADHAYA, A., & TIAN, Q., 1989. Evaluation of correlations for stagnant thermal conductivity of liquid-saturated porous beds of spheres, *International Journal of Heat Mass Transfer,* 32(9):1793-1796

REIMANN, J., PIAZZA, G. & HARSCH, H., 2006. Thermal conductivities of compressed beryllium pebbled beds, *Fusion Engineering and Design*, 81(7): 449-454

SLAVIN, A.J., ARCAS, V., GREENHALGH, C.A., IRVINE, E.R. & MARSHALL, D.B., 2002. Theoretical model for the thermal conductivity of a packed bed of solid spheroids in the presence of a static gas, with no adjustable parameters except at low pressure and temperature, *International Journal of Heat and Mass Transfer,* 45:4151-4161.

SLAVIN, A.J., LONDRY, F.A. & HARRISON, J., 2000. A new model for the effective thermal conductivity of packed beds of solid spheroids: alumina in helium between 100 and 500 °C, *International Journal of Heat and Mass Transfer,* 43:2059-2073

VAN ANTWERPEN, W., 2009. Modelling effective thermal conductivity in the near wall region of a packed pebble bed. North-West University.

VAN ANTWERPEN, W., DU TOIT, C.G. & ROUSSEAU, P.G., 2010. A review of correlations to model the packing structure and effective thermal conductivity in packed beds of mono-sized spherical particles, *Nuclear Engineering and Design*, 240:1803-1818.

VAN DER MEER, W.A., 2011. Private Communication.

VAN DER MERWE, J., MULDER, E.J. & VAN ANTWERPEN H.J., 2006. Heat transfer correlation limitations at the pebble bed-reflector interface, Proceedings HTR2006, October 1-4

VAN DER MERWE, J. & VAN RAVENSWAAY, J.P., 2003. Flownex Version 6.4 User Manual, M-Tech Industrial, Potchefstroom

WAKAO, N. & KATO, K., 1968. Effective thermal conductivity of packed beds, Journal of Chemical Engineering of Japan, 2:24-33.

YAGI, S. & KUNII, D., 1957. Studies on Effective Thermal Conductivities in Packed Beds, *A.I.Ch.E. Journal*, 3(3):373-381.

ZEHNER, P. & SCHLUENDER, E.U., 1970. Thermal conductivity of granular materials at moderate temperatures (German), Chemie-Ingr-Tech., 42:933.

ZHOU, Z.Y., YU, A.B. & ZULLI, P., 2010. A new computational method for studying heat transfer in fluid bed reactors, *Powder Technology*, 197:102-110.

www.en.wikipedia.org/wiki/Pebble_bed_reactor Date retrieved November 2011.

Appendix A

The Spherical Unit Nodalization model as programmed in EES:

The Long Range Radiation Effective Conductivity Calculations

Geometry

$d = 0.059$ [m] Diameter of a sphere

$d_c = 0.56$ [m] Inner diameter of the sphere control volume

Constants

$\sigma = 5.670E{-}08$ [W/m^2-K^4]

$\varepsilon = 0.8$

$A = \pi \cdot d^2$

$A_c = \pi \cdot d_c^2$

$A_1 = 0.0111876$ [m^2] Areas of the spheres within each ring

$A_2 = 0.0777826$ [m^2]

$A_3 = 0.0999984$ [m^2]

$A_4 = 0.266604$ [m^2]

$A_5 = 0.411139$ [m^2]

$A_6 = 0.587695$ [m^2]

$A_7 = 3.62473$ [m^2]

$A_8 = A_c$

$N = 7$ Number of rings

$NN = 8$ Number of rings + environment

$No_{s,i} = \frac{A_i}{A}$ for $i = 1$ to N No of spheres per ring

$A \cdot No_{s,i} \cdot F_{i,8} = Fac8_i$ for $i = 1$ to N Environmental ring view factors

$\sum_{j=1}^{NN} (F_{i,j}) = SF_i$ for $i = 1$ to N Test summation rule

$F_{j,i}$ = **Lookup** ('View Factors', i, J) for i = 1 to NN, j = 1 to N Assign view factors

$Q_8 = -1947$ [W]

$T_1 = 1462.15$ [K]

$Q_i = 0$ for i = 2 to N Heat boundaries in-between the rings

$$Q_i = \frac{E_{b,i} - J_i}{\frac{1-\varepsilon}{\varepsilon \cdot A_i}} \quad \text{for } i = 1 \text{ to } NN$$

$$E_{b,i} = \sigma \cdot T_i^4 \quad \text{for } i = 1 \text{ to } NN$$

For Surface 1:

$$\frac{E_{b,1} - J_1}{\frac{1-\varepsilon}{\varepsilon \cdot A_1}} = \frac{J_1 - J_2}{\frac{1}{A_1 \cdot F_{1,2}}} + \frac{J_1 - J_3}{\frac{1}{A_1 \cdot F_{1,3}}} + \frac{J_1 - J_4}{\frac{1}{A_1 \cdot F_{1,4}}} + \frac{J_1 - J_5}{\frac{1}{A_1 \cdot F_{1,5}}} + \frac{J_1 - J_6}{\frac{1}{A_1 \cdot F_{1,6}}} + \frac{J_1 - J_7}{\frac{1}{A_1 \cdot F_{1,7}}} + \frac{J_1 - J_8}{\frac{1}{A_1 \cdot F_{1,8}}}$$

For Surface 8:

$$\frac{E_{b,8} - J_8}{\frac{1-\varepsilon}{\varepsilon \cdot A_8}} = \frac{J_8 - J_1}{\frac{1}{Fac8_1}} + \frac{J_8 - J_2}{\frac{1}{Fac8_2}} + \frac{J_8 - J_3}{\frac{1}{Fac8_3}} + \frac{J_8 - J_4}{\frac{1}{Fac8_4}} + \frac{J_8 - J_5}{\frac{1}{Fac8_5}} + \frac{J_8 - J_6}{\frac{1}{Fac8_6}} + \frac{J_8 - J_7}{\frac{1}{Fac8_7}}$$

For Other Surfaces:

$$\frac{E_{b,i} - J_i}{\frac{1-\varepsilon}{\varepsilon \cdot A_i}} = \frac{J_i - J_1}{\frac{1}{A_i \cdot F_{i,1}}} + \frac{J_i - J_2}{\frac{1}{A_i \cdot F_{i,2}}} + \frac{J_i - J_3}{\frac{1}{A_i \cdot F_{i,3}}} + \frac{J_i - J_4}{\frac{1}{A_i \cdot F_{i,4}}} + \frac{J_i - J_5}{\frac{1}{A_i \cdot F_{i,5}}} + \frac{J_i - J_6}{\frac{1}{A_i \cdot F_{i,6}}} + \frac{J_i - J_7}{\frac{1}{A_i \cdot F_{i,7}}} + \frac{J_i - J_8}{\frac{1}{A_i \cdot F_{i,8}}}$$

Convert to Degree Celsius

$T_{c,i} = T_i - 273.15$ for i = 1 to NN

Lookup Table

View Factors

Paste Special	1 $RF_{1,i}$	2 $RF_{2,i}$	3 $RF_{3,i}$	4 $RF_{4,1}$	5 $RF_{5,i}$	6 $RF_{6,i}$	7 $RF_{7,i}$
Row 1	0.0000000	0.07206	0.03588	0.005431	0.0009305	0.0002013	0.0000125
Row 2	0.5009740	0.1714	0.1818	0.1041	0.02211	0.00451	0.000308
Row 3	0.3206680	0.2338	0.1576	0.09716	0.0683	0.01022	0.0006528
Row 4	0.1294230	0.357	0.259	0.2179	0.1711	0.1033	0.00596
Row 5	0.0341964	0.1169	0.2808	0.2639	0.2065	0.1756	0.03034
Row 6	0.0105754	0.03407	0.06005	0.2278	0.251	0.1927	0.07681
Row 7	0.0040421	0.01436	0.02366	0.08103	0.2675	0.4737	0.6231
Row 8	0.0001212	0.0005189	0.001115	0.002639	0.01253	0.03973	0.2628